nature neuroscience

ARTICLES

https://doi.org/10.1038/s41593-019-0524-y

A ventral CA1 to nucleus accumbens core engram circuit mediates conditioned place preference for cocaine

Yiming Zhou[1,2], Huiwen Zhu[1,2], Zhiyuan Liu[1,2], Xi Chen[1], XiuJuan Su[1], Chaonan Ma[1], Zhen Tian[1], Bing Huang[1], Enhui Yan[1], Xing Liu[1*] and Lan Ma[1*]

The importance of neuronal ensembles, termed engram cells, in storing and retrieving memory is increasingly being appreciated, but less is known about how these engram cells operate within neural circuits. Here we tagged engram cells in the ventral CA1 region of the hippocampus (vCA1) and the core of the nucleus accumbens (AcbC) during cocaine conditioned place preference (CPP) training and show that the vCA1 engram projects preferentially to the AcbC and that the engram circuit from the vCA1 to the AcbC mediates memory recall. Direct activation of the AcbC engram while suppressing the vCA1 engram is sufficient for cocaine CPP. The AcbC engram primarily consists of D1 medium spiny neurons, but not D2 medium spiny neurons. The preferential synaptic strengthening of the vCA1→AcbC engram circuit evoked by cocaine conditioning mediates the retrieval of cocaine CPP memory. Our data suggest that the vCA1 engram stores specific contextual information, while the AcbC D1 engram and its downstream network store both cocaine reward and associated contextual information, providing a potential mechanism by which cocaine CPP memory is stored.

Pioneering works have shown that the sparsely distributed neuron ensembles (that is, engram cells) can serve as the cellular representation of fear memory traces[1–4]. The engram cells in the dentate gyrus (DG) are preferentially reactivated following fear memory retrieval by related context exposure[5,6]. Ablation or inhibition of engram cells disrupts fear memory storage[7,8], while artificial activation of the memory engram by optogenetic or chemogenetic means induces the expression of fear in an irrelevant context or after retrograde amnesia caused through the interruption of consolidation or reconsolidation[6,9]. The critical role of engrams in memory storage and retrieval has been increasingly recognized[10,11].

Hebb's 'fire together, wire together' proposal hypothesized that the synchronously activated neurons can be recruited together and preferentially form a neural substrate of memory[12,13]. Several lines of evidence suggest that connections between engram cells within neural circuits may account for memory formation and retrieval of fear conditioning[9,14,15]. Electrophysiology and morphology data combined with optogenetic stimulation show that preferential connectivity of engram cell-to-engram cell within entorhinal cortex–DG–CA3 circuits is developed after fear conditioning. Long-term potentiation (LTP) is selectively induced in the conditional-stimulus-specific auditory pathways to engram cells in the lateral amygdala in auditory discriminative fear conditioning[16]. Optical silencing of CA1 engram cells impairs fear memory retrieval and inhibits engram cell activation in the amygdala and in the entorhinal, retrosplenial and perirhinal cortex[17]. However, intriguing questions remain regarding where the valence and related contextual information are allocated or encoded within the engram circuits, how the association of valence and contextual information are formed in the engram circuits, and how engram cells from different brain regions work collaboratively for storage of the associative memory. The organization of the engram network underlying associative memory storage remains poorly understood.

In this study, we use cocaine CPP, an associative memory model linking drug reward with neutral environment cues, to show that engram cells in the vCA1 project to engram cells in the AcbC, forming 'engram circuits' that store cocaine CPP memory and mediate its retrieval. The engram cells recruited in the AcbC are primarily dopamine receptor D1-expressing MSNs, not D2 MSNs. The vCA1 engram cells form preferential and strengthened connections to D1 engram neurons in the AcbC, and this postsynaptic strengthening is crucial for memory retrieval.

Results

Activation of cocaine engram cells in the AcbC and vCA1 is required for the retrieval of cocaine CPP memory. To identify the engram cells, c-fos-tTA×*tetO*-Cre×Ai14 mice were trained to associate cocaine reward (the valence information) with the context paired during training for the cocaine CPP (the contextual information). After the memory was acquired, mice were re-exposed to the CPP apparatus without giving cocaine, and this contextual-information-induced retrieval of cocaine CPP memory was assessed by measuring the time that the animal spent on the cocaine-paired side in the CPP apparatus. The preference for the cocaine-paired side indicates the expression of a reward-context associated memory. The cells activated during cocaine CPP conditioning in the absence of doxycycline (cocaine engram) were tagged by tdTomato expressed under the control of the *c-fos* promoter and a tetracycline-controlled transactivator (tTA), and activation of the cells by re-exposure to the CPP apparatus (test 1) was detected via c-Fos staining (Supplementary Fig. 1a,b). After cocaine CPP training,

[1]Department of Neurology, The State Key Laboratory of Medical Neurobiology and MOE Frontiers Center for Brain Science, School of Basic Medical Sciences, the Institutes of Brain Science, and Zhongshan Hospital, Fudan University, Shanghai, China. [2]These authors contributed equally: Yiming Zhou, Huiwen Zhu, Zhiyuan Liu. *e-mail: xingliu@fudan.edu.cn; lanma@fudan.edu.cn

engram cells tagged with tdTomato were detected in the AcbC, the vCA1, the prelimbic prefrontal cortex (PrL), the infralimbic prefrontal cortex and the basolateral amygdala (BLA) (Supplementary Fig. 1c). The reactivation of engram cells following re-exposure to the CPP apparatus, as demonstrated by increased c-Fos immunofluorescence in tdTomato-positive cells, was detected in the AcbC and the vCA1 (Supplementary Fig. 1d,e).

To test whether the retrieval of cocaine CPP memory is mediated by the activation of cocaine engram cells in these two brain nuclei, we expressed hM4D specifically in cocaine engram cells in the AcbC or the vCA1 (Fig. 1a). Silencing of either the AcbC or the vCA1 cocaine engram through the administration of clozapine *N*-oxide (CNO) impaired the expression of cocaine CPP memory during test 1 (Fig. 1b–d), which suggests that the activity of engram cells in the AcbC and the vCA1 is critically involved in the storage and/or retrieval of cocaine CPP memory. CNO did not affect the retrieval of cocaine CPP memory in C57BL/6 naive mice or in c-fos-tTA mice with mCherry expression in AcbC or vCA1 engram cells (Fig. 1c,d; Supplementary Fig. 2a,b). Chemogenetic interruption of the activation of either AcbC or vCA1 engram cells during test 1 did not significantly affect the CPP performance during test 2, which suggests that the stability of memory storage is not affected (Fig. 1c,d). Chemogenetic inhibition of the vCA1 or AcbC engram did not significantly change locomotor activity (Supplementary Fig. 2c–g).

vCA1 cocaine engram cells that project to the AcbC store distinct contextual information of cocaine CPP memory. The results of retrograde tracing with Fluorogold showed that the AcbC received direct innervation from the vCA1, the PrL, the ventral tegmental area (VTA) and the BLA (Supplementary Fig. 2h,i). To examine the role of the AcbC-projecting vCA1 engram in memory retrieval, we expressed eNpHR3.0 or hM4D in the vCA1 engram and manipulated the activity of the projection in the AcbC (Fig. 1e,f,h). Both optogenetic and chemogenetic inactivation of projection terminals of the vCA1 engram in the AcbC significantly reduced CPP scores in test 1, and the inhibitory effect was transient since it was not observed in test 2 (Fig. 1g,i). These results suggest that the context-induced retrieval of cocaine CPP memory depends on the activation of the AcbC projection of vCA1 engram cells.

Do these vCA1 engram cells encode specific cocaine-associated contextual information or, alternatively, are they, just like any other vCA1 neuron, generally required for the retrieval of any contextual memory? We examined the effects of inhibiting the vCA1 control engram not relevant to cocaine on the retrieval of cocaine CPP memory. We first tagged neurons that are activated in a neutral context with no association with cocaine (non-cocaine control engram) and then performed cocaine CPP training (Fig. 1j,k). As observed with cocaine CPP training, exposure to the neutral context induced comparable levels of neuronal activation in the vCA1 (Supplementary Fig. 3a,b), but, in contrast to the critical role of cocaine engram cells, chemogenetic inactivation of the non-cocaine control engram in the vCA1 had no effect on the retrieval of cocaine CPP memory (Fig. 1l), which suggests that the vCA1 engram cells encode specific contextual information for a distinct memory.

To further demonstrate the specificity of engram cells, we compared the activation of the non-cocaine control engram and the cocaine engram in the vCA1 via c-Fos staining after retrieval of cocaine CPP memory. The results showed that only 9% of the control engrams labeled in the neutral context in the vCA1 were activated (c-Fos$^+$mCherry$^+$/mCherry$^+$) in the cocaine CPP environment, which made up 12% of the total cells activated by retrieval (c-Fos$^+$mCherry$^+$/c-Fos$^+$). This value was significantly lower than the percentage of cocaine engram cells, therefore suggesting that retrieval of cocaine CPP memory specifically induces the activation of the cocaine engram (Supplementary Fig. 3c–f).

Next, we examined the proportions of vCA1 neurons projecting to their downstream regions by injecting the retrograde tracers CTB555, CTB488 and CTB647 into the AcbC, PrL and BLA, respectively. We observed that most of the vCA1 neurons were labeled by only one tracer, indicating that most vCA1 neurons exclusively send projections to and are dedicated to one of the three nuclei

Fig. 1 | Activation of the AcbC-projecting vCA1 engram is required for the retrieval of cocaine memory. a–d, c-fos-tTA mice were fed a diet containing doxycycline (Dox; 40 mg per kg) unless indicated otherwise. AAV TRE-tight-hM4D-mCherry was infused into the AcbC or vCA1 of c-fos-tTA mice. A regular diet, which did not contain doxycycline (no-Dox), was provided during cocaine-paired conditioning on days 2 and 3 to allow the c-fos-driven expression of hM4D-mCherry. CNO (1 mg per kg, i.p.) or saline was injected 30 min before test 1 on day 5, and memory retention was tested on day 6 (test 2). **a**, Experimental scheme. **b**, Left: CNO treatment (5 μM) decreased the action potential firing in response to a depolarizing current (100 pA) recorded from hM4D-expressing AcbC engrams. The experiment was independently repeated in 14 neurons from 7 mice per group, with similar results obtained. Middle: schematics of chemogenetic stimulation. Right: expression of hM4D-mCherry in the AcbC or vCA1 engram. The broken white line shows the position of anterior commissure (AC). The experiment was independently repeated, with similar results obtained in the mice for behavioral tests. **c**,**d**, Summary bar graphs of CPP scores. Two-way RM ANOVA. AcbC/hM4D: saline, $n=13$; CNO, $n=11$; $F_{\text{treatment}\times\text{session}}(2,44)=14.862$; $P=0.000012$. AcbC/mCherry: saline, $n=10$; CNO, $n=12$; $F_{\text{treatment}\times\text{session}}(2,40)=0.0751$; $P=0.928$. vCA1/hM4D: saline, $n=11$, CNO, $n=10$; $F_{\text{treatment}\times\text{session}}(2,38)=5.221$; $P=0.010$. vCA1/mCherry: saline, $n=10$; CNO, $n=11$; $F_{\text{treatment}\times\text{session}}(2,38)=1.465$; $P=0.244$. $^{***}P<0.001$ versus saline group. **e–i**, AAV TRE-tight-eNpHR3.0-eYFP or TRE-tight-hM4D-mCherry was infused into the vCA1 of c-fos-tTA mice. The no-Dox diet was provided during cocaine-paired conditioning and CPP was tested on day 5 (test 1, 5 min) and day 6 (test 2, 15 min). **e**, Experimental scheme. **f**,**h**, Left: schematics of photostimulation (**f**) or CNO infusion (**h**) in AcbC of c-fos-tTA mice. Representative voltage response evoked by 100 pA current injection showed that eNpHR3.0-expressing vCA1 engram cells were reponsive to photostimulation (593 nm, 2 mW, 2 s). Right: representative images of eNpHR3.0-eYFP (**f**) or hM4D-mCherry (**h**) fluorescence in the vCA1 engram and immunostaining with anti-eGFP (**f**) or anti-mCherry (**h**) antibody in their terminals in the AcbC. The broken white lines show the position of AC and optic fiber trace. The experiment was independently repeated with similar results in the mice for behavioral tests. **g**,**i**, Photostimulation (593 nm, 5 mW, 5 min) of AcbC was performed during test 1 (**g**) and CNO (3 μM, 200 nl per side) was infused into the AcbC 30 min before test 1 (**i**). The summary bar graphs present CPP scores for each minute. Two-way RM ANOVA. eNpHR3.0: eYFP, $n=14$; eNpHR3.0, $n=11$; $F_{\text{treatment}\times\text{session}}(2,46)=19.170$; $P=0.000001$ (**g**). hM4D: mCherry, $n=13$; hM4D, $n=9$; $F_{\text{treatment}\times\text{session}}(2,40)=7.514$; $P=0.002$ (**i**). $^{**}P<0.01$, $^{***}P<0.001$ versus eYFP or mCherry group. **j–l**, AAV TRE-tight-hM4D-mCherry was infused into the vCA1 of c-fos-tTA mice. The no-Dox diet was provided during a neutral context exposure (days −2 and −1) before cocaine CPP training. CNO (1 mg per kg, i.p.) or saline was injected 30 min before test 1. **j**, Experimental scheme. **k**, Schematic of chemogenetic stimulation (left) and representative images of hM4D-mCherry fluorescence in non-cocaine control engram cells in the vCA1 (right). The experiment was independently repeated with similar results in the mice for behavioral tests. **l**, Summary bar graphs of CPP scores. Two-way RM ANOVA. hM4D: saline, $n=12$; CNO, $n=10$; $F_{\text{treatment}\times\text{session}}(2,40)=0.250$; $P=0.780$. **m**, Average cell counts and Venn diagram illustrating the average proportions of vCA1 neurons projecting to the AcbC, PrL and BLA with retrograde tracer injection (AcbC, CTB555; PrL, CTB488; BLA, CTB647). $n=4$ mice. Scale bars, 100 μm. Bar graphs show the mean ± s.e.m. and individual data (circles).

(Fig. 1m). To assess the output specificity of the vCA1 cocaine engram, we tagged the vCA1 engram with eNpHR3.0-enhanced yellow fluorescent protein (eYFP) and excitatory neurons with channelrhodopsin 2 (ChR2)-mCherry, and estimated the extent of collateralization of vCA1 engram cells projecting to multiple downstream structures by measuring the eYFP intensity relative

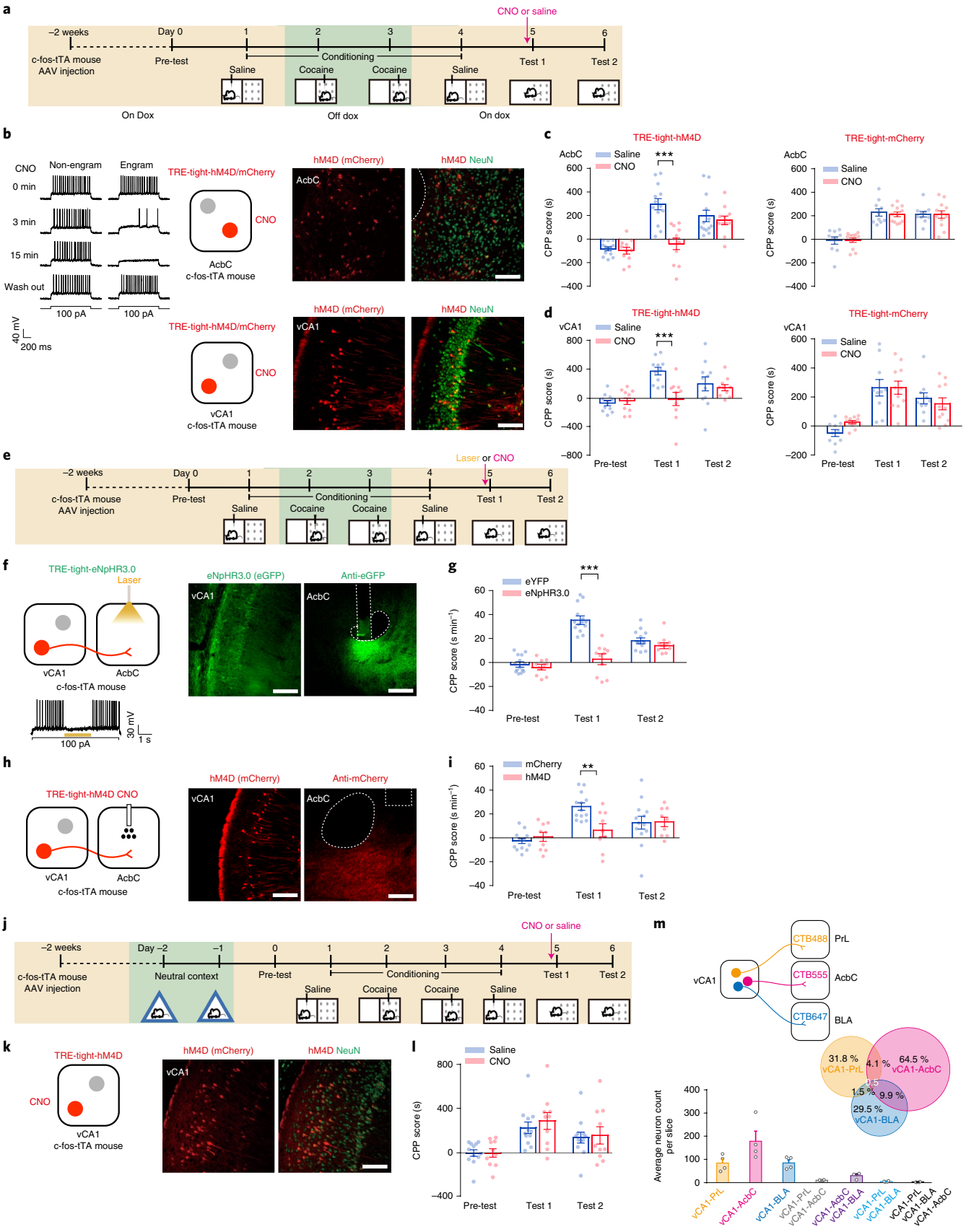

to the reference fluorescence (mCherry) (Supplementary Fig. 4a). The vCA1 cocaine engram and the control engram both sent collaterals to the Acb, the PrL and the amygdala (Supplementary Fig. 4b). The average green/red fluorescence ratio (engram/structure) in the cocaine engram group surpassed the control engram group in the Acb, but showed no difference in the PrL or the amygdala (Supplementary Fig. 4c).

Cocaine CPP memory storage depends on the vCA1→AcbC circuit composed of cocaine engram cells. To detect the functional connectivity from the vCA1 cocaine engram to the AcbC cocaine engram, we measured Ca^{2+} transients and c-Fos expression in the AcbC engram following activation of the vCA1 engram (Fig. 2a). The whole-cell electrophysiology results showed intact spike fidelity in response to laser stimulation (Fig. 2d). The in vivo optogenetic activation of ChR2-expressing cocaine engram cells in the vCA1 increased the GCaMP fluorescence levels of cocaine engram cells in the AcbC (Fig. 2b,c; Supplementary Fig. 5), and in vivo chemogenetic activation of the vCA1 engram increased c-Fos expression in the AcbC engram (Supplementary Fig. 6a–c). Moreover, we found that chemogenetic suppression of vCA1 engram activation during re-exposure to the CPP apparatus attenuated the activation of the AcbC engram (Supplementary Fig. 6d–f). These results indicate that the vCA1 engram is functionally connected to the AcbC engram and that activation of the AcbC engram, which is required for the expression of cocaine CPP memory, depends on activation of the vCA1 engram.

To verify whether the connection from the vCA1 engram to the AcbC engram plays a critical role in the storage and/or retrieval of cocaine CPP memory, we utilized the TRE3g-Cre/flex-taCasp3-TEVp system to induce Cre-dependent and caspase 3 (Casp3)-dependent apoptosis and to selectively ablate engram cells in the target brain nucleus. We co-expressed Casp3 and hM3D-mCherry in the AcbC engram. mCherry-positive cells were observed on day 5 after cocaine conditioning, whereas few of them could be detected on day 20, which indicates that AcbC engram cells had undergone Casp3-induced apoptosis (Fig. 2e,f,h). Consistently, cocaine CPP memory could be retrieved by re-exposure to the CPP test chamber on day 5 (test 1), but not on day 19 (test 2) (Fig. 2g,i). Moreover, the amnesia caused by apoptosis of AcbC engram cells could not be rescued by chemogenetic stimulation of either the vCA1 engram (Fig. 2h,i) or the AcbC engram (Fig. 2f,g) on day 20 (test 3). Chemogenetic activation of the vCA1 engram did not change the cocaine CPP score or locomotor activity (Supplementary Fig. 7). Similarly, photoactivation of ChR2-expressing vCA1 engram cells after transient inhibition of hM4D-expressing AcbC engram cells during test 1 failed to induce cocaine CPP expression (Fig. 2j–l). These results suggest that context-induced retrieval of cocaine CPP memory is dependent on an engram connection from the vCA1 to the AcbC.

Engram cells in the AcbC, but not the vCA1, are sufficient for CPP retrieval. We speculate that the vCA1 engram may encode cocaine-paired contextual information and that the AcbC engram may encode reward information of cocaine CPP memory. If this is true, direct activation of AcbC engram cells alone would retrieve cocaine reward memory, but not the contextual information it paired with, and thus the animal would not show preference to the cocaine-paired side when placed in the CPP apparatus. Our results showed that apoptosis (Fig. 3a–c) or chemogenetic inhibition (Fig. 3d–f) of the vCA1 engram resulted in a failure of memory retrieval. By contrast, chemogenetic activation of hM3D-expressing AcbC engram cells or photostimulation of ChR2-expressing AcbC engram cells could successfully induce the expression of cocaine CPP (Fig. 3c,f). In addition to optogenetic and chemogenetic activation of AcbC engram cells, we also presented mice with cocaine before re-exposure to the CPP box to activate AcbC neurons. Our data showed that cocaine injection could rescue the failure of cocaine CPP expression caused by the apoptosis of vCA1, but not AcbC, cocaine engram cells (Fig. 3g–l). Moreover, chemogenetic reactivation of the AcbC engram induced the expression of cocaine CPP in mice with amnesia caused by post-retrieval treatment with cycloheximide (Fig. 3m–o). These data indicate that independent of the vCA1, the cocaine engram in the AcbC networks encodes not only reward information but also the contextual information associated with cocaine reward.

The AcbC engram primarily consists of D1 MSNs. D1 and D2 MSNs are two major populations of projection neurons in the

Fig. 2 | The vCA1→AcbC engram circuits are required for cocaine memory storage. a–d, AAV TRE-ChR2-mCherry (ChR2) was infused into the vCA1, and AAVs TRE3g-Cre, DIO-GCaMP6s and hSyn-mCherry were infused into the AcbC of c-fos-tTA mice. An optical fiber was implanted in the vCA1 and AcbC, and GCaMP6s responses to photostimulation of the vCA1 were recorded on day 5. **a**, Experimental scheme. **b**, Left: schematic of virus injection, photostimulation and fluorescence recordings. Right: heatmaps illustrate the averaged mCherry or GCaMP fluorescence ($\Delta F/F$ %) in response to photostimulation of vCA1 engram (473 nm laser, a train of ten 15-ms light pulses at 20 Hz every 10 s for 15 min, blue vertical bars). Peri-event plots illustrate the averaged fluorescence. The curves and shaded regions indicate the mean ± s.e.m. $n = 7$ mice. **c**, The area under the curve (from −2 s to 10 s). Kruskal–Wallis one-way ANOVA on ranks, $n = 7$, $H = 9.800$ with 1 degree of freedom. $P = 0.002$. $^{**}P < 0.01$ versus mCherry. **d**, Action potential firing in response to patterned photostimulation (473 nm, 2 mW, 15-ms pulse width of 5 Hz, 10 Hz and 20 Hz for 1 s). The experiment was independently repeated in six neurons from two mice, with similar results obtained. **e–i**, AAVs TRE3g-Cre, Flex-taCasp3-TEVp and TRE-tight-hM3D-mCherry were infused into the AcbC or vCA1 of c-fos-tTA mice 2 weeks before the start of behavioral experiments. No-Dox food was provided during cocaine paired conditioning to allow c-fos-driven taCasp3 and hM3D-mCherry expression. CPP tests were performed on day 5 (test 1), day 19 (test 2) and day 20 (test 3). CNO (1 mg per kg, i.p.) was injected 30 min before test 3. **e**, Experimental scheme. **f**,**h**, Strategy for engram apoptosis and chemogenetic stimulation (left) and representative images of neuronal apoptosis in the AcbC and hM3D-mCherry expression in the AcbC or vCA1 on days 5 and 20 (right). The broken white lines show the position of AC. The experiment was independently repeated, with similar results obtained in five mice on day 5 and in the mice for behavioral tests on day 20. **g**,**i**, Summary bar graphs of CPP scores. Two-way RM ANOVA. hM3D, $n = 12$; hM3D/Casp3, $n = 11$; $F_{\text{treatment} \times \text{session}}(3,63) = 3.132$; $P = 0.032$ (**g**). hM3D, $n = 12$, hM3D/Casp3, $n = 11$; $F_{\text{treatment} \times \text{session}}(3,63) = 5.368$; $P = 0.002$ (**i**). $^{*}P < 0.05$, $^{***}P < 0.001$. **j–l**, AAV TRE-ChR2-mCherry was infused into the vCA1 and AAV TRE-tight-hM4D-mCherry was infused into the AcbC of c-fos-tTA mice. The no-Dox diet was provided during cocaine paired conditioning. CNO (1 mg per kg, i.p.) was injected 30 min before test 1, followed by photostimulation (473 nm laser, a train of ten 15-ms light pulses at 20 Hz every 10 s for 15 min) in the vCA1 during test 1. **j**, Experimental scheme. **k**, Schemetic of optical and chemogenetic stimulation (left) and the expression of ChR2-mCherry and hM4D-mCherry in the vCA1 and AcbC were as indicated (right). The broken white lines show the position of AC and optical fiber trace. The experiment was independently repeated, with similar results obtained in the mice for behavioral tests. **l**, Summary bar graphs of CPP scores. Two-way RM ANOVA. mCherry, $n = 13$; ChR2-mCherry, $n = 13$; $F_{\text{virus} \times \text{session}}(2,48) = 0.204$; $P = 0.816$. Scale bars, 100 μm. Bar graphs show the mean ± s.e.m. and individual data (circles).

AcbC; we therefore evaluated the activation of D1 and D2 MSNs after training and retrieval of cocaine CPP in D1-tdTomato and D2-enhanced green fluorescent protein (eGFP) reporter mice. As shown in Supplementary Fig. 8a–c, 79% of AcbC engram cells were D1 MSNs (c-Fos$^+$ tdTomato$^+$) and only 14% of AcbC engram cells were D2 MSNs (c-Fos$^+$ eGFP$^+$), while over 70% of cells activated

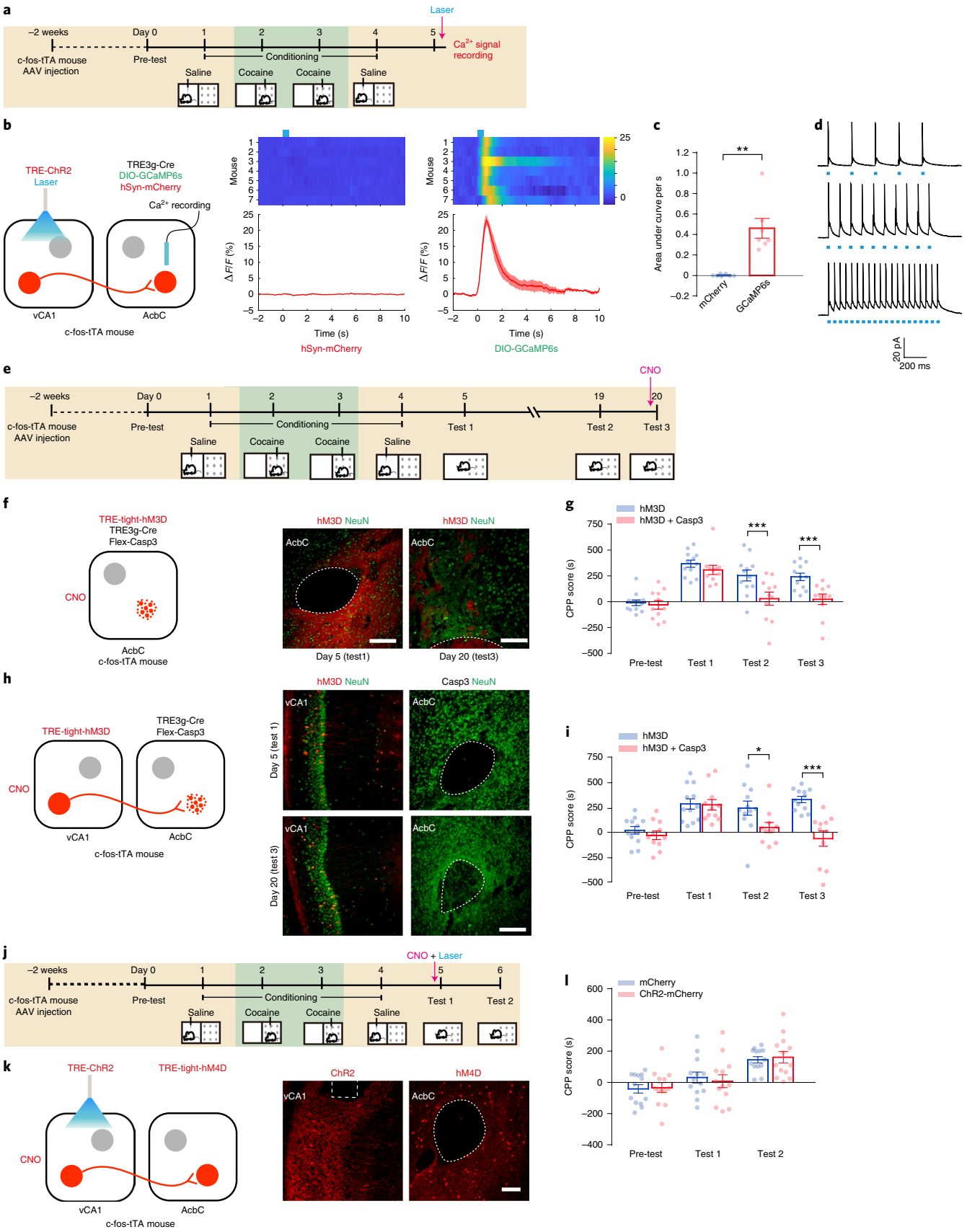

after memory retrieval were D1 MSNs (Supplementary Fig. 8d–h). The chemogenetic inhibition of D1 MSNs, but not D2 MSNs, in the AcbC impaired the retrieval of cocaine CPP memory (Fig. 4a–e). The chemogenetic activation of D1 MSNs in the AcbC increased the CPP score, while chemogenetic activation of D2 MSNs in the AcbC impaired the retrieval of cocaine CPP memory (Fig. 4f–i). The efficacy of CNO on the excitability of hM4D-expressing and hM3D-expressing AcbC D1 MSNs was verified ex vivo (Supplementary Fig. 8i–k).

We infected adeno-associated virus (AAV) DIO-WGA (double-*loxP*-flanked inverse open reading frame flanking wheat germ agglutinin) in the AcbC of D1-Cre and D2-Cre mice. More WGA-labeled cells were detected in the vCA1 of D1-Cre mice than in D2-Cre mice, which suggests that there is a preferential connection of vCA1 pyramidal neurons with D1 MSNs (Supplementary Fig. 9a–c). Data obtained using a retrograde rabies-virus-based input mapping system also revealed the presence of more dsRed$^+$ cells in the vCA1 of D1-Cre mice than in D2-Cre mice (Supplementary Fig. 9d–f). In addition, we injected anterograde self-complementary AAV (scAAV)-hSyn-Cre into the vCA1 of Ai14 mice and performed multiplexed single-molecule RNA fluorescence in situ hybridization (FISH) with *drd1*, *drd2* and *tdTomato* probes. The percentage of *drd1*$^+$ *tdTomato*$^+$ cells was significantly greater than *drd2*$^+$ *tdTomato*$^+$ cells (Supplementary Fig. 9g,h). These data suggest that D1 MSNs in the AcbC receive more inputs from the vCA1 than D2 MSNs.

Cocaine conditioning evokes synaptic remodeling at AcbC D1 engram neurons. Next, we investigated whether synaptic transmission in the engram cells is changed specifically after cocaine CPP training. The results showed that the frequency of miniature excitatory postsynaptic currents (mEPSCs) in randomly selected D1 and D2 MSNs did not change after saline conditioning, but mEPSC frequency was significantly increased primarily in D1 MSNs, but not D2 MSNs, after cocaine CPP training. Cocaine CPP training did not significantly change mEPSC amplitudes in D1 and D2 MSNs (Supplementary Fig. 10a–d). To investigate the synaptic changes in the AcbC engram, voltage-clamp recordings of randomly selected AcbC engram cells (H2B-GFP$^+$) and AcbC non-engram cells (H2B-GFP$^-$) were conducted (Supplementary Fig. 10e). The mEPSC amplitude and frequency of engram cells displayed a significant increase (Supplementary Fig. 10f–h) compared with those of non-engram cells. Given that our results revealed that AcbC engram cells are primarily D1 MSNs, the dendritic morphology and excitability of D1 engram and D1 non-engram neurons in the AcbC were quantified (Fig. 4j,k). D1 engram (H2B-GFP$^+$ H2B-mCherry$^+$) neurons in the AcbC had more mushroom and stubby types of spines than D1 non-engram (H2B-GFP$^+$ H2B-mCherry$^-$) neurons, while the total density of dendritic spines was not different. Moreover, the head diameter of mushroom-type spines in D1 engram neurons was also greater than that of D1 non-engram neurons (Fig. 4l,m). Next, the activity of AMPA receptors (AMPARs) at single synapses of D1 engram and D1 non-engram neurons was examined using whole-cell patch-clamp recording (Fig. 4n). D1 engram neurons showed increased mEPSC amplitude, but not frequency, compared with D1 non-engram neurons (Fig. 4o,p), which suggests that there is an increased AMPAR response at synapses of D1 engram neurons in the AcbC.

Cocaine conditioning preferentially strengthens the synaptic connectivity of the vCA1→AcbC engram circuit. To assess afferent-specific glutamatergic synaptic transmission in the vCA1→AcbC cocaine engram circuit, the paired-pulse ratio (PPR) and the AMPAR/NMDA receptor (NMDAR) (A/N) ratio of evoked EPSCs in randomly selected AcbC D1 engram (H2B-GFP$^+$ H2B-mCherry$^+$) and D1 non-engram (H2B-GFP$^+$ H2B-mCherry$^-$) cells after photostimulation of axon terminals of

Fig. 3 | Activation of the AcbC engram retrieves cocaine CPP memory independent of the vCA1 engram. a–c, AAVs TRE3g-Cre and Flex-taCasp3-TEVp were infused into the vCA1, and AAV TRE-tight-hM3D-mCherry was infused into the AcbC of c-fos-tTA mice 2 weeks before the start of behavioral experiments. No-Dox food was provided during conditioning to allow c-fos-driven hM3D-mCherry and taCasp3 expression. CPP tests were performed on day 5 (test 1), day 19 (test 2) and day 20 (test 3). CNO (1 mg per kg, i.p.) was injected 30 min before test 3. **a**, Experimental scheme. **b**, Strategy for engram apoptosis and chemogenetic stimulation (left) and representative images of hM3D-mCherry expression in the AcbC and neuronal apoptosis in the vCA1 on days 5 and 20 (right). The broken white lines show the position of AC. The experiment was independently repeated, with similar results obtained in five mice on day 5 and in the mice for behavioral tests on day 20. **c**, Summary bar graph of CPP scores. Two-way RM ANOVA. hM3D, $n=12$; hM3D/Casp3, $n=11$; $F_{\text{treatment}\times\text{session}}(3,63)=6.307$; $P=0.000825$. $^{***}P<0.001$. **d–f**, AAV TRE-ChR2-mCherry was infused into the AcbC, and AAV TRE-tight-hM4D-mCherry was infused into the vCA1 of c-fos-tTA mice. No-Dox food was provided during conditioning. CNO (1 mg per kg, i.p.) was injected 30 min before test 1, followed by photostimulation (473 nm laser, a train of ten 15-ms light pulses at 20 Hz every 10 s for 15 min) in the AcbC during test 1. **d**, Experimental scheme. **e**, Schematic of optic and chemogenetic stimulation (left) and the expression of ChR2-mCherry in the AcbC and hM4D-mCherry in the vCA1 were as indicated (right). The broken white lines show the position of AC and optic fiber trace. The experiment was independently repeated, with similar results obtained in the mice for behavioral tests. **f**, Summary bar graphs of CPP scores. Two-way RM ANOVA. mCherry, $n=15$; ChR2-mCherry, $n=17$; $F_{\text{treatment}\times\text{session}}(2,60)=7.797$; $P=0.000977$. $^{***}P<0.001$. **g–l**, AAVs TRE3g-Cre and Flex-taCasp3-TEVp were infused into the AcbC (**h–j**) or vCA1 (**k** and **l**) of c-fos-tTA mice 2 weeks before the start of the behavioral experiments. No-Dox food was provided during conditioning to allow c-fos-driven taCasp3 expression in the engram. CPP tests were performed on day 5 (test 1), day 19 (test 2) and day 20 (test 3). Cocaine (15 mg per kg, i.p.) was injected before test 3. **g**, Experimental scheme. **h**,**k**, Strategy for engram apoptosis (left) and representative images of NeuN immunofluorescence in the AcbC or vCA1 (right; samples taken after test 3 or the last behavioral test). The broken white lines show the position of AC. The experiment was independently repeated, with similar results obtained in the mice for behavioral tests. **i**,**l**, Summary bar graphs of CPP scores in tests 1–3. Two-way RM ANOVA. mCherry, $n=14$; Casp3, $n=14$; $F_{\text{treatment}\times\text{session}}(3,78)=3.126$; $P=0.031$(**i**). Control (Ctrl), $n=10$; Casp3, $n=14$; $F_{\text{treatment}\times\text{session}}(3,66)=3.865$; $P=0.013$ (**l**). $^{**}P<0.01$, $^{***}P<0.001$. **j**, After test 3, mice were given a second round of cocaine CPP training, and were tested for CPP on days 21 (pre-test II) and 26 (test II). Summary bar graphs of CPP scores in pre-test II and test II are shown. Two-way RM ANOVA. Ctrl, $n=14$; Casp3, $n=14$; $F(1,26)=40.095$; $P=0.000001$. $^{***}P<0.001$. **m–o**, AAV TRE-tight-hM3D-mCherry was infused into the AcbC of c-fos-tTA mice 2 weeks before behavioral experiments. The no-Dox diet was provided during cocaine paired conditioning. CPP was tested on day 6 (test 1) and day 7 (test 2). Cycloheximide (CHX; 60 mg per kg, s.c.) or saline was given immediately after retrieval (5 min). CNO (1 mg per kg, i.p.) was injected 30 min before test 2. **m**, Experimental scheme. **n**, Schematics of chemogenetic stimulation (left) and representative images of hM3D-mCherry expression in the AcbC (right). The broken white lines show the position of AC. The experiment was independently repeated, with similar results obtained in the mice for behavioral tests. **o**, Summary bar graph of CPP scores. Friedman's two-way RM ANOVA by ranks. Saline, $n=9$; CHX, $n=7$; $F_{\text{treatment}\times\text{session}}(1,14)=6.854$; $P=0.020$. $^{*}P<0.05$. Scale bars, 100 μm. Bar graphs show the mean ± s.e.m. and individual data (circles).

ChR2-expressing vCA1 excitatory or vCA1 engram neurons were determined in brain slices containing the AcbC (Fig. 5a,d). The PPR and A/N ratio of evoked EPSCs recorded in AcbC D1 engram and D1 non-engram neurons did not differ after optogenetic stimulation of axon terminals of vCA1 excitatory neurons in the AcbC (Fig. 5b,c). The result of selective photostimulation

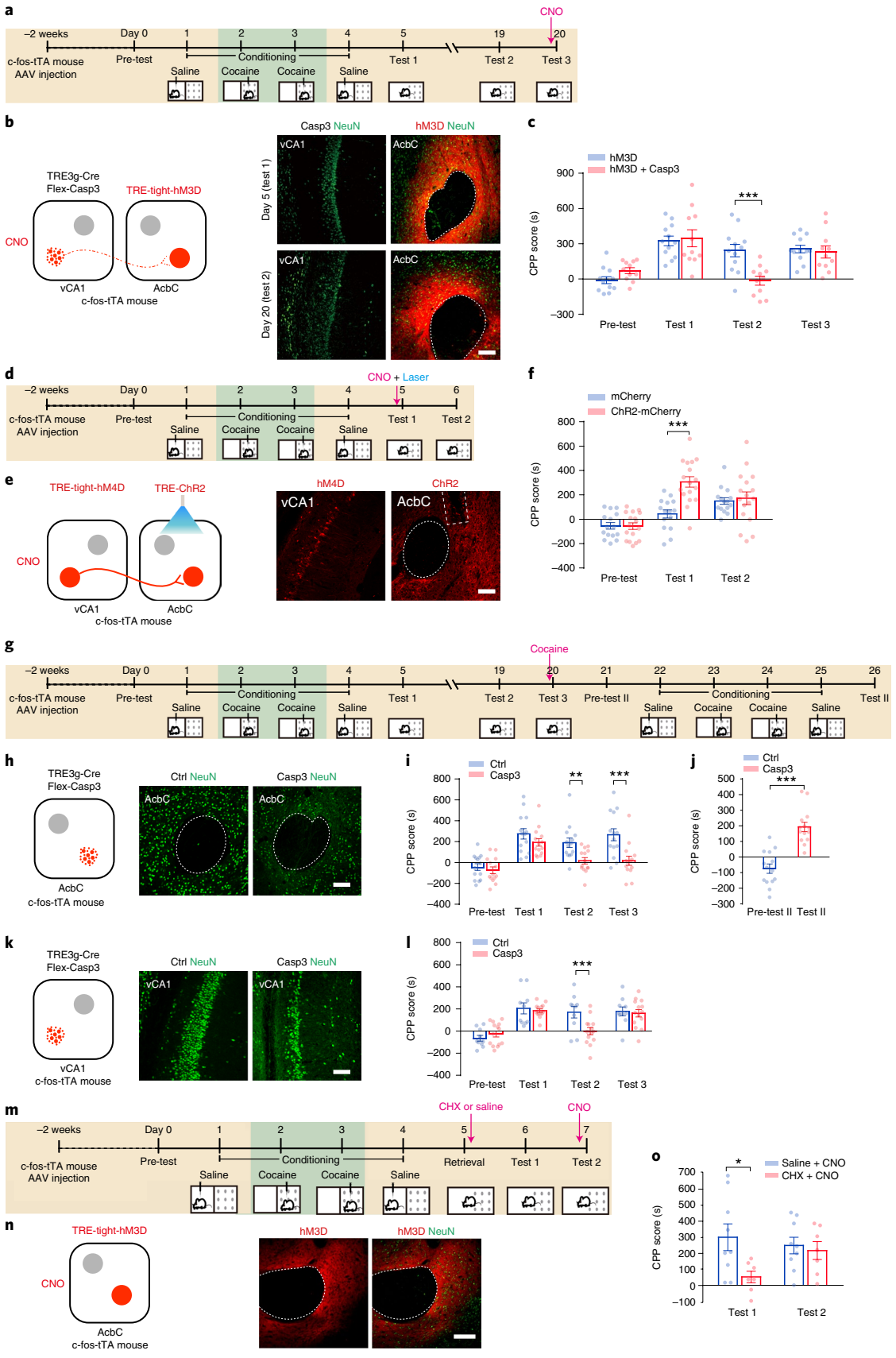

of vCA1 engram axons in the AcbC also revealed no difference in the PPR of evoked EPSCs between AcbC D1 engram and D1 non-engram neurons (Fig. 5e,f). However, the average A/N ratio of evoked EPSCs in AcbC D1 engram cells was significantly higher than that of D1 non-engram neurons (Fig. 5g). Selective photoactivation of the axon of the vCA1 non-cocaine control engram in the AcbC did not affect the PPR or the A/N ratio of D1 engram and D1 non-engram neurons (Supplementary Fig. 11a–c). In addition, following photostimulation of vCA1 engram projections, the D2 engram showed a similar PPR and A/N ratio to D2 non-engram neurons (Supplementary Fig. 11d–f). These data indicate that the probability of glutamate release from the terminals of vCA1 engram neurons to AcbC D1 engram neurons was similar to AcbC D1 non-engram neurons, but the activity of synaptic glutamate receptors was specifically enhanced in AcbC D1 engram neurons compared with AcbC D1 non-engram neurons. These data suggest that acquisition of cocaine CPP memory is associated with the formation of a vCA1→AcbC engram circuit with enhanced glutamatergic synaptic efficacy, and that the engram-specific plasticity changes occur preferentially in the AcbC D1 engram at the presynaptic input from vCA1 engram, likely conveying cocaine-associated contextual information to the AcbC D1 engram.

The results above suggest that after cocaine conditioning, the vCA1→AcbC engram circuit undergoes long-lasting synaptic strengthening, including altered postsynaptic AMPARs. To confirm whether the input-specific synaptic remodeling in the AcbC engram is necessary for memory expression, we introduced long-term depression (LTD) and LTP in the vCA1→AcbC engram circuit to reduce or enhance postsynaptic AMPARs[18–20] and to change synaptic strengthening. Low-frequency photostimulation (LFS) of ChR2-expressing axons of the vCA1 engram in the AcbC was conducted in vivo[21] 40 min before testing (Fig. 6a,b). This process significantly inhibited the retrieval of cocaine CPP memory (Fig. 6c), whereas it did not affect locomotion and anxiety levels (Supplementary Fig. 12). High-frequency photostimulation (HFS) was then carried out 1 day before test 3 (Fig. 6g,h). HFS of oChIEF-expressing axons of the vCA1 engram in the AcbC after extinction training reinstated cocaine CPP (Fig. 6i). The efficacy of LFS and HFS was validated. In vivo LFS of vCA1 engram terminals in the AcbC significantly decreased the A/N ratio in D1 engram cells (Fig. 6d,e). In vivo HFS of vCA1 engram terminals significantly increased the A/N ratio in D1 engram cells compared with the HFS untreated group. Under HFS, the A/N ratio of D1 engram cells was higher than that of D1 non-engram cells (Fig. 6j,k). These data indicate that brief stimulation of the vCA1–AcbC engram projection at 1 Hz or 100 Hz successfully induced LTP or LTD in AcbC engram cells. The PPR remained unchanged after HFS, but increased after LFS (Fig. 6f,l). These data suggest that vCA1-engram-input-specific synaptic strengthening in the AcbC engram is a representation of coding for cocaine-context association.

Discussion

The critical roles of engram cells in memory are increasingly being recognized. However, with regard to the mechanisms of memory storage, where the valence and related contextual information is encoded in engram circuits and how engram connectivity changes contribute to memory coding and recall remain largely unknown. In this study, we utilized cocaine CPP, a model of associative memory of drug reward and related context, to demonstrate that the cocaine engram cells in the vCA1 and the AcbC are required for the storage and retrieval of cocaine CPP memory. Our data suggest that the vCA1 engram preferentially projects to the AcbC and encodes distinct contextual information, and that the AcbC engram stores cocaine reward and associated context information. Cocaine CPP conditioning evokes vCA1-engram-input-specific postsynaptic remodeling of the AcbC D1 engram that underlies the storage of cocaine CPP memory.

The AcbC in limbic neural circuits is responsible for reward and goal-directed behaviors[22]. The reinforcement and reward of addictive drugs are related to dopamine innervation from the VTA to the AcbC, and goal-directed behaviors are regulated by glutamate projections that originate in limbic frontal cortical regions, including the BLA, the ventral hippocampus and the medial prefrontal cortex, which converge on spiny neurons of the AcbC[23]. The AcbC[24], the BLA[25], the dorsal hippocampus[26] and the VTA[27] are key brain nuclei for the formation or retrieval of the memory of drug reward. In this

Fig. 4 | Cocaine CPP training induces synaptic potentiation of AcbC D1 engram cells. a–i, AAVs DIO-hM4D-mCherry or DIO-hM3D-mCherry were infused into the AcbC of D1-Cre or D2-Cre mice 2 weeks before the start of behavioral experiments. CPP tests were performed on day 4 (test 1) and day 5 (test 2). CNO (1 mg per kg, i.p.) was injected 30 min before test 1. Conditioning was done using 15 mg per kg cocaine, except for **g**, in which data were acquired after conditioning with 5 mg per kg cocaine. **a**, Experimental scheme. **b**,**d**,**f**,**h**, Schematics of chemogenetic stimulation (left) and representative images of hM4D-mCherry or hM3D-mCherry expression in D1 MSNs and D2 MSNs in the AcbC of D1-Cre and D2-Cre mice (right). The broken white lines show the position of AC. The experiment was independently repeated, with similar results obtained in the mice for behavioral tests. Scale bar, 100 μm. **c**,**e**,**g**,**i**, Summary bar graphs of CPP scores. Two-way RM ANOVA. Saline, $n=11$; CNO, $n=14$; $F_{\text{treatment}\times\text{session}}(2,46)=5.736$; $P=0.006$ (**c**). Saline, $n=11$; CNO, $n=11$; $F_{\text{treatment}\times\text{session}}(2,40)=0.0475$; $P=0.954$ (**e**). Saline, $n=10$; CNO $n=9$; $F_{\text{treatment}\times\text{session}}(2,34)=3.305$; $P=0.049$ (**g**). Saline, $n=13$; CNO, $n=11$; $F_{\text{treatment}\times\text{session}}(2,44)=3.602$; $P=0.036$ (**i**). $^{*}P<0.05$, $^{**}P<0.01$, $^{***}P<0.001$. **j**–**p**, AAVs c-fos-tTA, TRE3g-H2B-mCherry and DIO-H2B-GFP were infused into the AcbC of D1-Cre mice. No-Dox food was provided during cocaine conditioning. Morphological and electrophysiological analyses were performed on day 5. **j**, Experimental scheme. **k**, Schematics of virus injection and electrophysiological recordings (left) and representative fluorescence images of the D1 engram (H2B-GFP^{+} H2B-mCherry^{+}) and the D1 non-engram (H2B-GFP^{+} H2B-mCherry^{-}) cells (right). The experiment was independently repeated in three mice, with similar results obtained. Scale bar, 50 μm. **l**, Representative images of dendritic spines by infusion of lucifer yellow into D1 engram (H2B-GFP^{+} H2B-mCherry^{+}) and D1 non-engram (H2B-GFP^{+} H2B-mCherry^{-}) cells. The lower panels are images of the area outlined in red in the upper panels. The experiment was independently repeated, with similar results obtained in all the neurons in **m**. Scale bar, 30 μm (top) and 5 μm (bottom). **m**, Density and head diameter of spines of D1 engram and D1 non-engram cells. One-way RM ANOVA or Kruskal–Wallis one-way ANOVA on ranks. D1 engram, $n=34$ neurons from 6 mice; D1 non-engram, $n=26$ neurons from 6 mice. Total spine density: $F(1,58)=2.635$, $P=0.110$. Mushroom density: $F(1,58)=18.639$, $P=0.000062$. Stubby density: $H=5.768$ with 1 degree of freedom, $P=0.016$. Thin density: $H=0.200$ with 1 degree of freedom, $P=0.654$. Mushroom diameter: $H=4.679$ with 1 degree of freedom, $P=0.031$. Thin diameter: $H=0.006$ with 1 degree of freedom, $P=0.941$. $^{*}P<0.05$, $^{**}P<0.01$, $^{***}P<0.001$. **n**, Representative traces of mEPSC recordings of AcbC D1 engram and D1 non-engram cells. The experiment was independently repeated, with similar results obtained in all the neurons in **o** and **p**. **o**,**p**, Plots and summary bar graphs of mEPSC amplitude (**o**) and frequency (**p**). Two-tailed Student's *t*-test. D1 non-engram, $n=18$ neurons from 7 mice; D1 engram, $n=19$ neurons from 7 mice. $t(35)=-2.954$, $P=0.006$ (amplitude); $t(35)=-0.605$, $P=0.549$ (frequency); Kolmogorov–Smirnov test, cumulative probability of the amplitude: $P<0.000001$; cumulative probability of the inter-event intervals: $P=0.331$. $^{**}P<0.01$. Bar graphs show the mean ± s.e.m. and individual data (circles).

study, we found that the inhibition or ablation of AcbC engram cells prevented the expression of cocaine CPP memory. Direct activation of AcbC engram cells after post-retrieval treatment with cycloheximide restored the preference for the cocaine-paired side. Moreover, chemogenetic activation after apoptosis of AcbC engram cells failed to rescue the expression of cocaine CPP memory. These data indicate that the AcbC engram is critical for the retrieval and/or storage of cocaine CPP memory.

The differential responses of D1 and D2 MSNs to cocaine have been reported by many laboratories. The basal level of activity of D1 MSNs is much lower than D2 MSNs in the Acb, and acute cocaine administration enhances the activity and c-Fos expression in D1 MSNs and suppresses D2 MSN activity[28,29]. Repeated cocaine exposure increases the mEPSC frequency of D1 MSNs[30]. Cocaine conditioning increases the calcium transients in D1 MSNs and decreases them in D2 MSNs, and following cocaine CPP retrieval, D1 MSNs show an increase in Ca^{2+} transient just seconds before mice cross into the cocaine-paired context, whereas a decreased activity of D2 MSNs occurs after entry[28]. During re-exposure to the CPP box, the putative D2 MSNs fire more when the animals stay in

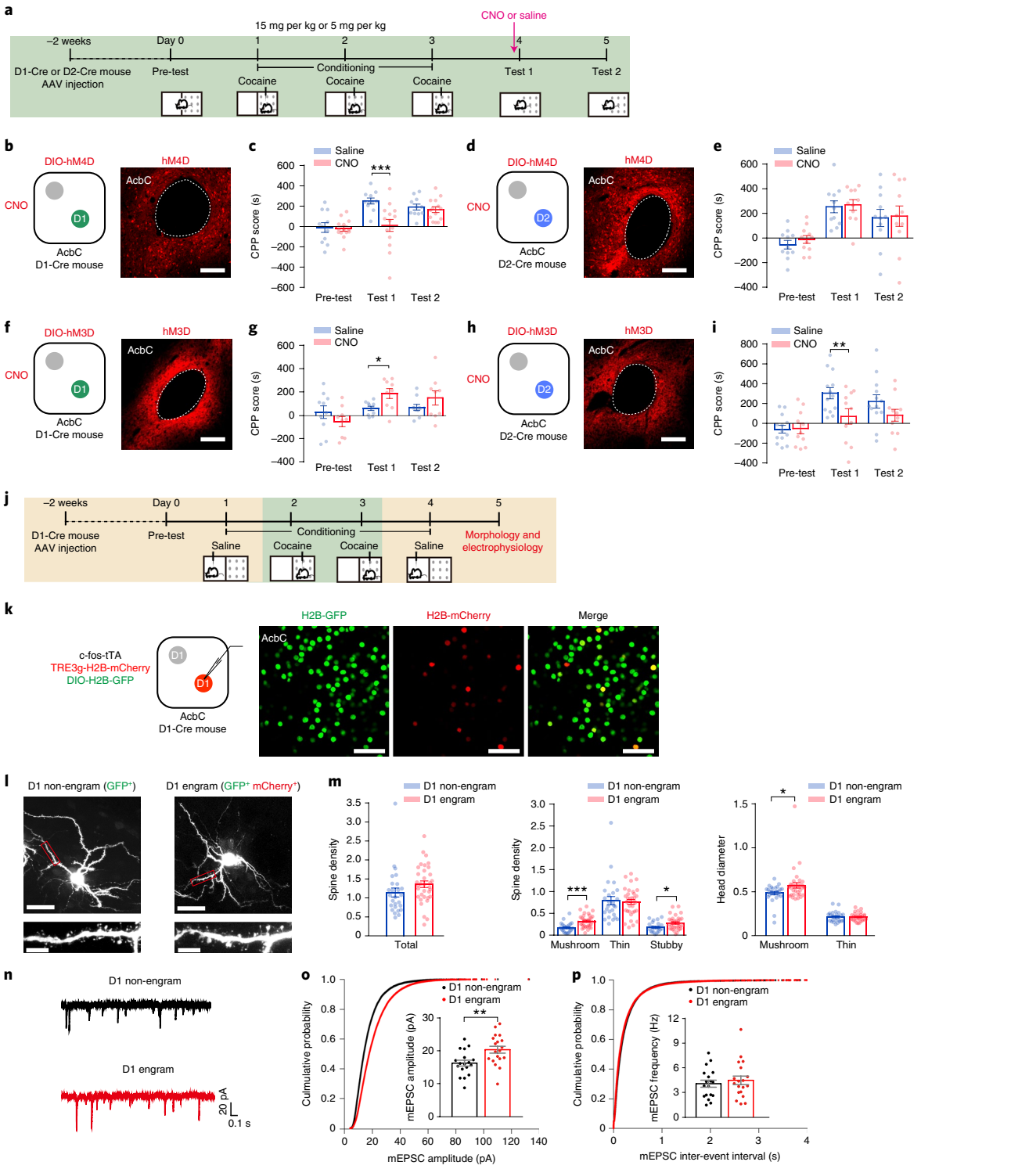

the cocaine zone than when they stay in the saline zone[31]. In this study, we showed that inhibition of D1 MSNs, but not D2 MSNs, in the AcbC impaired the retrieval of cocaine CPP memory, while activation of D1 MSNs and D2 MSNs promoted and impaired, respectively, the retrieval of cocaine CPP memory. These results are consistent with a previous study[32] that showed that optogenetic activation of D1 and D2 MSNs oppositely regulate cocaine reward. We further demonstrate that the majority of neurons activated by CPP retrieval are D1 MSNs, which implicates that D1 engram cells in the AcbC play a critical role in the retrieval of cocaine CPP memory. The pivotal role of MSNs and their plasticity in different cocaine-related behaviors are known[33]; however, the relationship between the change in firing rates of MSNs and plasticity as well as adaptation in behavior is yet to be understood. The functional significance of activation of D2 MSNs (for example, spiking rate change), synaptic plasticity and interactions with D1 MSNs during and post-cocaine CPP training are interesting directions for further investigation.

Our results indicate a critical role of D1 engram cells in encoding cocaine CPP memory. These engram neurons may encode positive valence information of CPP. The increased time spent in a previously cocaine-paired chamber could also be explained by other factors, for example, salience, familiarity or increased motivation to seek the drug[34,35]; therefore, it is also possible that Acb engram cells encode other information or its combination with reward. In this study, we showed that terminal inhibition of AcbC projections of the vCA1 engram impaired context-induced retrieval of cocaine CPP memory. Silencing vCA1 engram cells led to a selective reduction in the reactivation of AcbC engram cells and failure of memory retrieval, while activation of vCA1 engram cells after apoptosis or inhibition of AcbC engram cells failed to induce cocaine CPP expression. These results suggest that AcbC inputs of the vCA1 engram may store contextual information that is critical for the natural recall of cocaine CPP memory. Moreover, we showed that selective activation of AcbC engram cells by chemogenetic and optogenetic methods after apoptosis or silencing of the vCA1 engram cells could successfully retrieve CPP memory. These data indicate that direct activation of AcbC engram cells, in the absence of the vCA1 engram, is sufficient for CPP expression. Cocaine can increase local dopamine concentrations and activate D1 MSNs in the Acb[36,37]. We also gave mice cocaine before re-exposure to the CPP box, and found that cocaine could rescue the failure of cocaine CPP expression caused by the apoptosis of vCA1, but not AcbC, cocaine engram cells. Our results therefore suggest that the contextual representations are not exclusive to the vCA1 engram. Instead, a cellular representation of contextual information appears to have been concurrently established in the AcbC and its downstream network during memory acquisition. A previous study[38] showed that optogenetic stimulation of a specific neural ensemble in the retrosplenial cortex is sufficient to produce freezing behavior in a neutral context independent of the dorsal hippocampus. Our study proposes the possibility that engram cells in the Acb or other brain nuclei may also store the contextual information in addition to the vCA1, so that the AcbC alone is capable of sustaining memory trace and mediating the retrieval of cocaine CPP memory.

The idea that the efficacy changes of synapses within diverse neural circuits may mediate memory storage has long been posited. The theoretical hypotheses about the remodeling of synaptic plasticity as the substrate of memory and the circumstances in which such changes take place date back to Santiago Ramon y Cajal[39], Donald Hebb[40] and Jerzy Konorski[41].However, a 40-year-old question still remains: how does synaptic plasticity mediate distinct memory? In this study, we compared D1 engram cells and D1 non-engram cells in the AcbC and observed that AcbC D1 engram cells show significantly increased dendritic spine density and EPSCs relative to D1 non-engram cells. The A/N ratio of AcbC D1 engram neurons was higher than that of D1 non-engram neurons following optogenetic stimulation of vCA1 engram axons, therefore indicating that vCA1-engram-specific LTP was preferentially induced in AcbC D1 engram cells. To verify whether this increased plasticity at the AcbC engram represents mnemonic information, we examined the effect of selectively reducing or enhancing postsynaptic AMPARs in AcbC engram neurons on memory retrieval through the optogenetic induction of LTD or LTP in the vCA1→AcbC engram circuit. Our data showed that synaptic depression of the vCA1→AcbC engram circuit before retrieval suppressed memory expression, and synaptic potentiation of these engram circuits reinstated cocaine CPP memory after extinction training. After cocaine CPP training, engram neurons in the AcbC and the vCA1 undergo c-fos-driven transcriptional activation, which leads to morphological and functional plasticity changes in the vCA1→AcbC engram circuit. The preferential

Fig. 5 | Cocaine CPP training preferentially increases the synaptic connectivity from the vCA1 engram to AcbC D1 engram cells. a–c, AAVs c-fos-tTA, TRE3g-H2B-mCherry and DIO-H2B-GFP were infused into the AcbC, and the AAV CaMKIIα:ChR2-mCherry was infused into the vCA1 of D1-Cre mice. No-Dox food was provided during cocaine paired conditioning. On day 5, electrophysiological recording of D1 engram (H2B-GFP$^+$ H2B-mCherry$^+$) and D1 non-engram (H2B-GFP$^+$ H2B-mCherry$^-$) cells in the AcbC was performed on brain slices. **a**, Experimental scheme (left) and schematic of photostimulation and electrophysiological recordings (right). **b**,**c**, Representative traces in response to photostimulation (473 nm laser, 1-ms pulse width, blue vertical bar) on axon terminals of ChR2-expressing vCA1 excitatory cells in the AcbC and summary bar graphs of PPR (**b**) and A/N ratio (**c**) in D1 engram and D1 non-engram cells. Kruskal–Wallis one-way ANOVA on ranks or one-way ANOVA. PPR (50 ms), $n = 32$ D1 non-engram neurons from 7 mice; $n = 41$ D1 engram neurons from 7 mice; $H = 0.119$ with 1 degree of freedom; $P = 0.730$. PPR (100 ms), $n = 28$ D1 non-engram neurons from 7 mice; $n = 33$ D1 engram neurons from 7 mice; $F(1,59) = 0.0315$; $P = 0.860$. A/N, $n = 27$ D1 non-engram neurons from 7 mice; $n = 26$ D1 engram neurons from 7 mice; $F(1,51) = 2.606$; $P = 0.113$. **d–g**, AAVs c-fos-tTA, TRE3g-H2B-mCherry and DIO-H2B-GFP were infused into the AcbC, and AAVs c-fos-tTA and TRE-ChR2-mCherry were infused into the vCA1 of D1-Cre mice. No-Dox food was provided during cocaine conditioning. On day 5, electrophysiological recording of AcbC D1 engram (H2B-GFP$^+$ H2B-mCherry$^+$) and D1 non-engram (H2B-GFP$^+$ H2B-mCherry$^-$) cells were performed on slices. **d**, Experimental scheme (left) and schematic of photostimution and electrophysiological recordings (right). **e**, The expression of ChR2-mCherry in vCA1 engram cells, H2B-mCherry in AcbC engram cells and H2B-GFP in D1 MSNs. The experiment was independently repeated in three mice, with similar results obtained. Scale bars, 50 μm. **f**,**g**, Representative traces (top) and quantification (bottom) of PPRs (**f**) and A/N ratios (**g**) in AcbC D1 non-engram and D1 engram cells recorded after photostimulation (473 nm laser, 5-ms pulse width, blue vertical bar) of ChR2-expressing axon terminals of vCA1 engram cells in the AcbC. Kruskal–Wallis one-way ANOVA on ranks or one-way ANOVA. PPR (50 ms), $n = 20$ D1 non-engram neurons from 9 mice; $n = 20$ D1 engram neurons from 9 mice; $H = 0.003$ with 1 degree of freedom; $P = 0.957$. PPR (100 ms), $n = 21$ D1 non-engram neurons from 11 mice; $n = 26$ D1 engram neurons from 11 mice; $F(1,45) = 0.002$; $P = 0.967$. A/N, $n = 17$ D1 non-engram neurons from 12 mice; $n = 21$ D1 engram neurons from 12 mice; $F(1,36) = 6.585$; $P = 0.015$. $^{**}P < 0.01$. Bar graphs show the mean ± s.e.m. and individual data (circles).

connectivity of the neuronal assemblies distributed across the vCA1 and the AcbC is established during learning and thereby provides a specific substrate for cocaine reward memory storage, and adds new evidence for a correlation between memory storage and synaptic potentiation. Our data support the hypothesis that cocaine-conditioning-induced synaptic remodeling of the vCA1→AcbC engram circuit represents the information encoding of cocaine reward and reward-associated context. More importantly, these findings indicate the physically wired engram circuits for drug memory storage and retrieval[42].

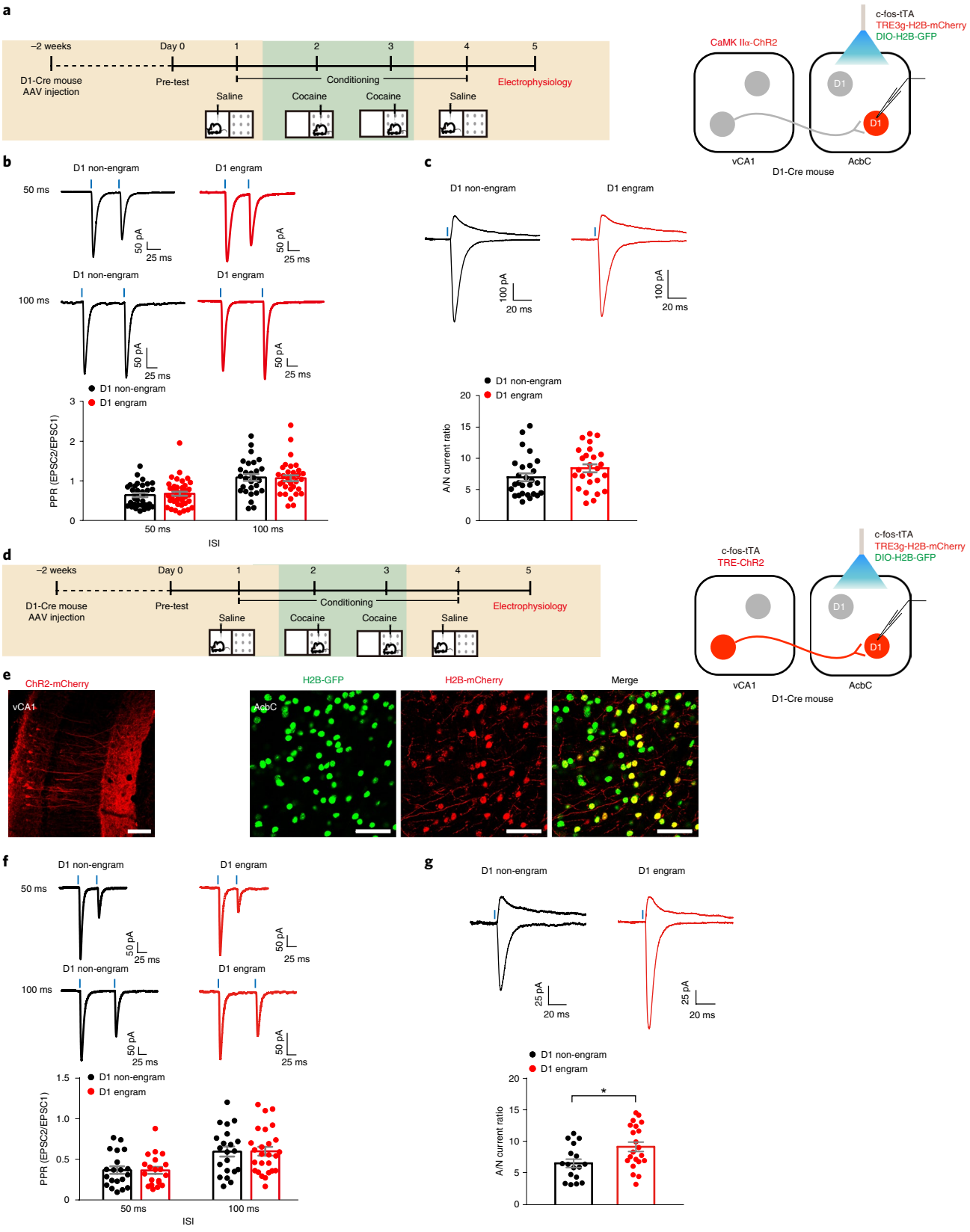

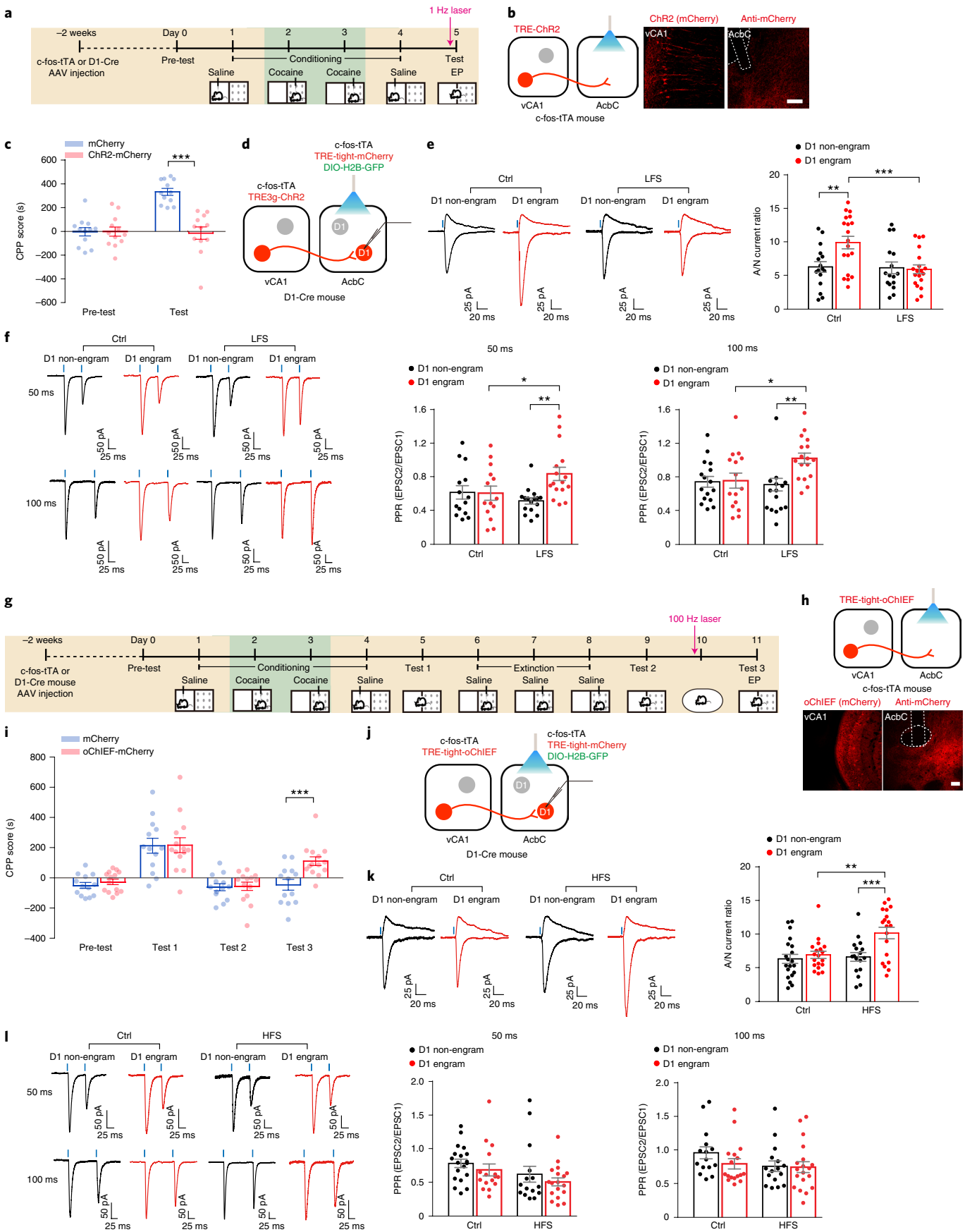
a
1 Hz laser
–2 weeks
Day 0
1
2
3
4
5
c-fos-tTA or D1-Cre AAV injection
Pre-test
Conditioning
Test
Saline
Cocaine
Cocaine
Saline
EP
b
TRE-ChR2
vCA1
AcbC
c-fos-tTA mouse
ChR2 (mCherry)
Anti-mCherry
c
mCherry
ChR2-mCherry
***
CPP score (s)
Pre-test
Test
d
c-fos-tTA
TRE-tight-mCherry
DIO-H2B-GFP
c-fos-tTA
TRE3g-ChR2
D1
vCA1
AcbC
D1-Cre mouse
e
Ctrl
LFS
D1 non-engram
D1 engram
25 pA
20 ms
D1 non-engram
D1 engram
**
***
A/N current ratio
Ctrl
LFS
f
Ctrl
LFS
D1 non-engram
D1 engram
50 ms
100 ms
50 pA
25 ms
50 ms
100 ms
D1 non-engram
D1 engram
*
**
PPR (EPSC2/EPSC1)
Ctrl
LFS
g
100 Hz laser
–2 weeks
Day 0
1
2
3
4
5
6
7
8
9
10
11
c-fos-tTA or D1-Cre mouse AAV injection
Pre-test
Conditioning
Test 1
Extinction
Test 2
Test 3
EP
Saline
Cocaine
Cocaine
Saline
Saline
Saline
Saline
Saline
h
TRE-tight-oChIEF
vCA1
AcbC
c-fos-tTA mouse
oChIEF (mCherry)
Anti-mCherry
i
mCherry
oChIEF-mCherry
***
CPP score (s)
Pre-test
Test 1
Test 2
Test 3
j
c-fos-tTA
TRE-tight-oChIEF
c-fos-tTA
TRE-tight-mCherry
DIO-H2B-GFP
D1
vCA1
AcbC
D1-Cre mouse
k
Ctrl
HFS
D1 non-engram
D1 engram
25 pA
20 ms
D1 non-engram
D1 engram
**
***
A/N current ratio
Ctrl
HFS
l
Ctrl
HFS
D1 non-engram
D1 engram
50 ms
100 ms
50 pA
25 ms
50 ms
100 ms
D1 non-engram
D1 engram
PPR (EPSC2/EPSC1)
Ctrl
HFS

Fig. 6 | LFS of vCA1→AcbC engram circuits inhibits and HFS promotes the retrieval of cocaine CPP memory. a–c, AAV TRE3g-ChR2-mCherry was infused into the vCA1 of c-fos-tTA mice. No-Dox food was provided during cocaine paired conditioning. On day 5, LFS (473-nm laser, 4 ms, 10 min, 1 Hz, 18–20 mW) was delivered into the AcbC 40 min before testing. **a**, Experimental scheme. EP, electrophysiology. **b**, Schematic of photostimulation (left) and representative images of ChR2-mCherry expression in vCA1 engram cells and their terminals in the AcbC stained with antibody against mCherry (right). The broken white lines show the position of AC and optic fiber trace. The experiment was independently repeated, with similar results obtained in the mice for behavioral tests. **c**, Summary bar graphs of CPP scores. Two-way RM ANOVA. mCherry, $n=12$; ChR2-mCherry, $n=12$; $F_{\text{virus}\times\text{session}}(1,22)=30.595$; $P=0.000015$. $^{***}P<0.001$. **d–f**, AAVs c-fos-tTA, TRE-tight-mCherry and DIO-H2B-GFP were infused into the AcbC, and AAVs c-fos-tTA and TRE3g-ChR2-mCherry were infused into the vCA1 of D1-Cre mice. On day 5, LFS was delivered in the AcbC and brain slices were prepared for electrophysiological recordings 40 min later. **d**, Schematic of photostimulation and electrophysiological recordings. **e**,**f**, Representative traces in response to photostimulation (473-nm laser, 5-ms pulse width, blue vertical bar) on axon terminals of ChR2-expressing vCA1 engram cells in AcbC containing slices prepared 40 min after LFS and quantification of A/N ratios (**e**) and PPRs (**f**) in D1 engram and D1 non-engram cells. Two-way ANOVA without adjustments. A/N: Ctrl, $n=16$ D1 non-engram neurons and $n=19$ D1 engram neurons from 5 mice. LFS: $n=16$ D1 non-engram neurons and 19 D1 engram neurons from 6 mice; $F_{\text{treatment}\times\text{cell type}}(1,66)=5.475$; $P=0.022$. PPR (50 ms): Ctrl, $n=14$ D1 non-engram neurons and $n=14$ D1 engram neurons from 5 mice; LFS, $n=16$ D1 non-engram neurons and $n=16$ D1 engram neurons from 6 mice; $F_{\text{treatment}\times\text{cell type}}(1,56)=5.330$; $P=0.025$. PPR (100 ms): Ctrl, $n=16$ D1 non-engram neurons and $n=15$ D1 engram neurons from 5 mice; LFS, $n=15$ D1 non-engram neurons and $n=17$ D1 engram neurons from 6 mice; $F_{\text{treatment}\times\text{cell type}}(1,59)=4.258$; $P=0.043$. $^{*}P<0.05$, $^{**}P<0.01$, $^{***}P<0.001$. **g–i**, AAV TRE-tight-oChIEF-mCherry was infused into the vCA1 of c-fos-tTA mice. A no-Dox diet was provided during cocaine conditioning. Extinction learning was performed on days 6–8. CPP tests were performed on day 5 (test 1), day 9 (test 2) and day 11 (test 3). HFS (473-nm laser, 6 trains of 100× 2-ms pulses given at 100 Hz with 20 s inter-train-interval, 18–20 mW) was delivered into the AcbC 1 day before test 3. **g**, Experimental scheme. EP, electrophysiology. **h**, Schematics of photostimulation (top) and representative images of oChIEF-mCherry expression in vCA1 engram cells and their terminals in the AcbC stained with antibody against mCherry (bottom). The broken white lines show the position of AC and optic fiber trace. The experiment was independently repeated, with similar results obtained in the mice for behavioral tests. **i**, Summary bar graphs of CPP scores. Friedman's two-way RM ANOVA by ranks. mCherry, $n=13$; oChIEF-mCherry, $n=14$; $F_{\text{virus}\times\text{session}}(3,75)=4.700$; $P=0.005$. $^{***}P<0.001$. **j–l**, AAVs c-fos-tTA, TRE-tight-mCherry, and DIO-H2B-GFP were infused into the AcbC, and AAVs c-fos-tTA and TRE-tight-oChIEF-mCherry were infused into the vCA1 of D1-Cre mice. **j**, Schematic of photostimulation and electrophysiological recordings. **k**,**l**, Representative traces in response to photostimulation (473-nm laser, 5-ms pulse width, blue vertical bar) on axon terminals of oChIEF-expressing vCA1 engram cells in AcbC-containing slices prepared 1 day after HFS and quantification of A/N ratios (**k**) and PPRs (**l**) in D1 engram and D1 non-engram cells. Two-way ANOVA without adjustments. A/N: Ctrl, $n=20$ D1 non-engram neurons and $n=19$ D1 engram neurons from 5 mice; HFS: $n=17$ D1 non-engram neurons and $n=19$ D1 engram neurons from 6 mice; $F_{\text{treatment}\times\text{cell type}}(1,71)=4.584$, $P=0.036$. PPR (50 ms): Ctrl, $n=19$ D1 non-engram neurons and $n=16$ D1 engram neurons from 5 mice; HFS: $n=15$ D1 non-engram neurons and $n=18$ D1 engram neurons from 6 mice; $F_{\text{treatment}\times\text{cell type}}(1,64)=0.010$; $P=0.920$. PPR (100 ms): Ctrl, $n=15$ D1 non-engram neurons and $n=17$ D1 engram neurons from 5 mice; HFS, $n=16$ D1 non-engram neurons and $n=19$ D1 engram neurons from 6 mice; $F_{\text{treatment}\times\text{cell type}}(1,63)=0.855$, $P=0.359$. $^{**}P<0.01$ versus the indicated group. Scale bars, 100 μm. Bar graphs show the mean ± s.e.m. and individual data (circles).

Online content

Any methods, additional references, Nature Research reporting summaries, source data, extended data, supplementary information, acknowledgements, peer review information, details of author contributions and competing interests, and statements of code and data availability are available at https://doi.org/10.1038/s41593-019-0524-y.

Received: 18 October 2018; Accepted: 23 September 2019;
Published online: 12 November 2019

References

1. Tonegawa, S., Liu, X., Ramirez, S. & Redondo, R. Memory engram cells have come of age. *Neuron* **87**, 918–931 (2015).
2. Josselyn, S. A. Continuing the search for the engram: examining the mechanism of fear memories. *J. Psychiatry Neurosci.* **35**, 221–228 (2010).
3. Reijmers, L. G., Perkins, B. L., Matsuo, N. & Mayford, M. Localization of a stable neural correlate of associative memory. *Science* **317**, 1230–1233 (2007).
4. Tonegawa, S., Morrissey, M. D. & Kitamura, T. The role of engram cells in the systems consolidation of memory. *Nat. Rev. Neurosci.* **19**, 485–498 (2018).
5. Denny, C. A. et al. Hippocampal memory traces are differentially modulated by experience, time, and adult neurogenesis. *Neuron* **83**, 189–201 (2014).
6. Liu, X. et al. Optogenetic stimulation of a hippocampal engram activates fear memory recall. *Nature* **484**, 381–385 (2012).
7. Zhou, Y. et al. CREB regulates excitability and the allocation of memory to subsets of neurons in the amygdala. *Nat. Neurosci.* **12**, 1438–1443 (2009).
8. Han, J. H. et al. Selective erasure of a fear memory. *Science* **323**, 1492–1496 (2009).
9. Ryan, T. J., Roy, D. S., Pignatelli, M., Arons, A. & Tonegawa, S. Memory. Engram cells retain memory under retrograde amnesia. *Science* **348**, 1007–1013 (2015).
10. Josselyn, S. A., Kohler, S. & Frankland, P. W. Finding the engram. *Nat. Rev. Neurosci.* **16**, 521–534 (2015).
11. Tonegawa, S., Pignatelli, M., Roy, D. S. & Ryan, T. J. Memory engram storage and retrieval. *Curr. Opin. Neurobiol.* **35**, 101–109 (2015).
12. Lowel, S. & Singer, W. Selection of intrinsic horizontal connections in the visual cortex by correlated neuronal activity. *Science* **255**, 209–212 (1992).
13. Munakata, Y. & Pfaffly, J. Hebbian learning and development. *Dev. Sci.* **7**, 141–148 (2004).
14. Roy, D. S., Muralidhar, S., Smith, L. M. & Tonegawa, S. Silent memory engrams as the basis for retrograde amnesia. *Proc. Natl Acad. Sci. USA* **114**, E9972–E9979 (2017).
15. Choi, J. H. et al. Interregional synaptic maps among engram cells underlie memory formation. *Science* **360**, 430–435 (2018).
16. Kim, W. B. & Cho, J. H. Encoding of discriminative fear memory by input-specific LTP in the amygdala. *Neuron* **95**, 1129–1146 e1125 (2017).
17. Tanaka, K. Z. et al. Cortical representations are reinstated by the hippocampus during memory retrieval. *Neuron* **84**, 347–354 (2014).
18. Huganir, R. L. & Nicoll, R. A. AMPARs and synaptic plasticity: the last 25 years. *Neuron* **80**, 704–717 (2013).
19. Diering, G. H., Gustina, A. S. & Huganir, R. L. PKA-GluA1 coupling via AKAP5 controls AMPA receptor phosphorylation and cell-surface targeting during bidirectional homeostatic plasticity. *Neuron* **84**, 790–805 (2014).
20. Kessels, H. W. & Malinow, R. Synaptic AMPA receptor plasticity and behavior. *Neuron* **61**, 340–350 (2009).
21. Bagot, R. C. et al. Ventral hippocampal afferents to the nucleus accumbens regulate susceptibility to depression. *Nat. Commun.* **6**, 7062 (2015).
22. Nicola, S. M. The nucleus accumbens as part of a basal ganglia action selection circuit. *Psychopharmacology* **191**, 521–550 (2007).
23. Pignatelli, M. & Bonci, A. Role of dopamine neurons in reward and aversion: a synaptic plasticity perspective. *Neuron* **86**, 1145–1157 (2015).
24. Joseph, M. H., Datla, K. & Young, A. M. The interpretation of the measurement of nucleus accumbens dopamine by in vivo dialysis: the kick, the craving or the cognition? *Neurosci. Biobehav. Rev.* **27**, 527–541 (2003).
25. Miller, C. A. & Marshall, J. F. Molecular substrates for retrieval and reconsolidation of cocaine-associated contextual memory. *Neuron* **47**, 873–884 (2005).
26. Otis, J. M., Fitzgerald, M. K. & Mueller, D. Inhibition of hippocampal beta-adrenergic receptors impairs retrieval but not reconsolidation of cocaine-associated memory and prevents subsequent reinstatement. *Neuropsychopharmacology* **39**, 303–310 (2014).

27. Degoulet, M., Stelly, C. E., Ahn, K. C. & Morikawa, H. L-type Ca^{2+} channel blockade with antihypertensive medication disrupts VTA synaptic plasticity and drug-associated contextual memory. *Mol. Psychiatry* **21**, 394–402 (2016).
28. Calipari, E. S. et al. In vivo imaging identifies temporal signature of D1 and D2 medium spiny neurons in cocaine reward. *Proc. Natl Acad. Sci. USA* **113**, 2726–2731 (2016).
29. Bertran-Gonzalez, J. et al. Opposing patterns of signaling activation in dopamine D1 and D2 receptor-expressing striatal neurons in response to cocaine and haloperidol. *J. Neurosci.* **28**, 5671–5685 (2008).
30. Kim, J., Park, B. H., Lee, J. H., Park, S. K. & Kim, J. H. Cell type-specific alterations in the nucleus accumbens by repeated exposures to cocaine. *Biol. Psychiatry* **69**, 1026–1034 (2011).
31. Sjulson, L., Peyrache, A., Cumpelik, A., Cassataro, D. & Buzsaki, G. Cocaine place conditioning strengthens location-specific hippocampal coupling to the nucleus accumbens. *Neuron* **98**, 926–934.e5 (2018).
32. Lobo, M. K. et al. Cell type-specific loss of BDNF signaling mimics optogenetic control of cocaine reward. *Science* **330**, 385–390 (2010).
33. Graziane, N. M. et al. Opposing mechanisms mediate morphine- and cocaine-induced generation of silent synapses. *Nat. Neurosci.* **19**, 915–925 (2016).
34. Tzschentke, T. M. Measuring reward with the conditioned place preference (CPP) paradigm: update of the last decade. *Addict. Biol.* **12**, 227–462 (2007).
35. Sun, Y., Chen, G., Zhou, K. & Zhu, Y. A conditioned place preference protocol for measuring incubation of craving in rats. *J. Vis. Exp.* https://doi.org/10.3791/58384 (2018).
36. Dong, Y. et al. Cocaine-induced potentiation of synaptic strength in dopamine neurons: behavioral correlates in *GluRA*$^{-/-}$ mice. *Proc. Natl Acad. Sci. USA* **101**, 14282–14287 (2004).
37. Di Chiara, G. & Imperato, A. Drugs abused by humans preferentially increase synaptic dopamine concentrations in the mesolimbic system of freely moving rats. *Proc. Natl Acad. Sci. USA* **85**, 5274–5278 (1988).
38. Cowansage, K. K. et al. Direct reactivation of a coherent neocortical memory of context. *Neuron* **84**, 432–441 (2014).
39. Jones, E. G. Santiago Ramon y Cajal and the Croonian lecture, March 1894. *Trends Neurosci.* **17**, 190–192 (1994).
40. Morris, R.G. D.O. Hebb: The Organization of Behavior, Wiley: New York; 1949. *Brain Res. Bull.* **50**, 437 (1999).
41. Konorski, J. Mechanisms of learning. *Sym. Soc. Exp. Biol.* **4**, 408–431 (1950).
42. Liu, X. et al. β-Arrestin-biased signaling mediates memory reconsolidation. *Proc. Natl Acad. Sci. USA* **112**, 4483–4488 (2015).

Methods

Animals. The following animals were used in this study: C57BL/6 mice from the Shanghai Laboratory Animal Center, CAS; c-fos-tTA (018306) and *Gt(ROSA)26Sor*$^{tm14(CAG-tdTomato)Hze}$ (Ai14, 007914) mice from The Jackson Laboratory; and D1-Cre (034258-UCD), D2-Cre mice (032108-UCD) and D2-eGFP BAC transgenic mice (036931-UCD) from The Mutant Mouse Resource and Research Center. D1-tdTomato mice were obtained by cross-breeding D1-Cre with Ai14 mice. Animals were housed four per cage and kept on a reversed 12 h light–dark cycle with ad libitum food and water. Male mice (8–10 weeks old) were used for the behavioral experiments. Experimental procedures were performed in accordance with the National Institutes of Health *Guide for the Care and Use of Laboratory Animals* and were approved by the Animal Care and Use Committee of the Shanghai Medical College of Fudan University.

CPP test. The CPP apparatus consisted of two compartments (15 × 15 × 20 cm^3) with different flooring and walls separated by a removable board. One compartment had black and white striped walls, a white floor with or without frosted stripes and a black ceiling. The other compartment had black and white checkered walls, a black floor and a white ceiling. Behavioral subjects were individually habituated to the investigator by handling for 5 min and placed in the experimental environment for adaptation for 3 days before the CPP session. A standard cocaine CPP protocol[42] was applied, including a pre-test, conditioning and a retention test. During the pre-test phase, mice were released from the middle of the conditioning apparatus and allowed to freely explore the full extent of the CPP apparatus for 15 min. The sessions were video-recorded and the time spent in each chamber was determined. Mice that spent >65% (>585 s) or <35% (<315 s) of the total time (900 s) in one side were eliminated from subsequent CPP experiments. After behavioral labeling, mice were randomly assigned to either the experimental or the control group.

For engram labeling experiments using c-fos-tTA mice, the conditioning phase included four successive days with one conditioning trial each day. Conditioning was conducted on mice confined to one chamber for 30 min paired with a saline injection (4 ml per kg, intraperitoneally (i.p.)) on days 1 and 4, and on mice confined to another chamber for 30 min paired with a cocaine injection (15 mg per kg, i.p.) on days 2 and 3. For the retention test, mice were released from the middle part of the CPP apparatus and allowed to freely explore both chambers for 5 min or 15 min. For experiments using C57BL/6 mice, we used alternative two daily conditioning sessions over 3 days, which lasted 30 min each. The mice were injected with cocaine (15 mg per kg) or saline (4 ml per kg) on alternating morning and afternoon sessions with a 6-h interval and repeated for 3 days. Photostimulation was performed during the entire test phase. For chemogenetic stimulation, CNO was injected i.p. (1 mg per kg) or locally into the AcbC (3 μM, 0.2 μl) 30 min before the memory retention test. For the expression of taCasp3-TEVp experiment, retention tests were conducted 2 weeks after the first retention test. The memory retention tests were performed as indicated. The retention phases were taped using a digital video camera, and a trained observer blinded to the genotype and treatment group recorded the time that the mice spent exploring the two chambers according to the video using a stopwatch. The CPP score was calculated by subtracting the duration spent within the saline-paired side from the cocaine-paired side.

Preparation of AAVs. The pAAV-TRE-mCherry, pAAV-TRE-eYFP and pAAV-TRE-ChR2-mCherry plasmids were gifts from S. Tonegawa (RIKEN-MIT Center). The pAAV-hsyn:WGA-Cre plasmid was a gift from M. Luo (National Institute of Biological Sciences, China). The AAV-EF1α:FLEx-taCasp3-TEVp plasmid was a gift from J. Hu (ShanghaiTech University, China). The AAV-hSyn:DIO-WGA plasmid was modified in our laboratory. An AAV preparation titer of 2×10^{12} vector genome per ml was used. AAV2-hsyn:WGA-Cre, AAV2-EF1α:DIO-hM4D-mCherry and AAV2-EF1α:DIO-hM3D-mCherry were generated by and acquired from the University of North Carolina at Chapel Hill Vector Core. AAV9-hsyn:DIO-GCaMP6s-eGFP, AAV9-TRE3g-Cre, AAV9-TRE3g-histone-mCherry, AAV9-TRE3g-ChR2-mCherry, AAV9-TRE-tight-hM4D-mCherry, AAV9-TRE-tight-hM3D-mCherry, AAV9-hsyn:DIO-histone-eGFP, AAV9-EF1α:DIO-his-eGFP−2a-TVA, AAV9-EF1α:DIO-RVG and RV-ENVA-*delta*G-dsRed (RV*d*G; 5.0×10^8 colony forming units per ml) were generated and packaged by BrainVTA. AAV9-TRE-ChR2-mCherry, AAV8-EF1α:hM4D-mCitrine, AAV8-EF1α:DIO-hM4D-GFP and AAV8-c-fos-tTA were packaged by Neuron Biotech. AAV9-CaMKIIα:ChR2-mCherry, AAV9-hsyn:DIO-WGA, AAV9-TRE-tight-eNpHR3.0-eYFP, AAV9-TRE-tight-eYFP, AAV9-TRE-tight-oChIEF-mCherry, AAV9-TRE-tight-mCherry and scAAV2/1-hSyn:Cre were generated and packaged by Taitool Biological. AAV2-EF1α:FLEx-taCasp3-TEVp was generated and packaged by Genechem.

Stereotaxic surgery. For virus injection, 6-week-old mice were anesthetized with isoflurane (3.5% induction, 1.5–2% maintenance), placed in a stereotaxic apparatus (Stoelting Instruments) and injected (50 nl min^{-1}) with small amounts of AAV (150–200 nl) in the specific brain area, including the AcbC, the vCA1, the PrL and the BLA, with a 10-μl syringe and a 36-gauge blunt needle under the control of a UMP3 ultra micropump (World Precision Instruments). The needle was slowly lowered to the target site and remained for at least 5 min after the injection. The incision was closed with sutures. For optical fiber implantation, a jewelry screw was placed on the skull close to the implant site of each hemisphere to provide additional stability. A layer of dental cement was applied to secure the optical fiber implant with a sleeve for protection. Mice remained on a heating pad until fully recovered from anesthesia and given Baytril (10 mg per kg, subcutaenously (s.c.)) twice a day for 3 days. Following surgery, the mice were allowed to recover and housed for 2–3 weeks before behavioral experiments, histological analyses or ex vivo electrophysiological recordings.

AAVs were bilaterally delivered to the following brain regions (coordinates relative to Bregma in parentheses): AcbC (anterior–posterior (AP): +1.6 mm; medial–lateral (ML): ±1.2 mm; dorsal–ventral (DV): −4.3 mm; vCA1 (AP: −3.5 mm; ML: ±3.7 mm; DV: −3.7 mm); PrL (AP: +1.8 mm; ML: ±0.3 mm; DV: −2.8 mm); or BLA (AP: −1.5 mm; ML: ±3.3; DV: −4.8). For optogenetic experiments, ceramic fiber optic cannulas (200 μm in diameter, 0.37 numerical aperture (NA), Anilab Software & Instruments) were implanted bilaterally above the AcbC (AP: +1.6 mm; ML: ±1.7 mm; DV: −4.0 mm, 10° angle) or the vCA1 (AP: −3.5 mm; ML: ±3.7 mm; DV: −3.5 mm). For photometry experiments, ceramic fiber optic cannulas (200 μm in diameter, 0.48 NA, Hangzhou Newdoon Technology) were implanted ipsilaterally in the AcbC (ML: 1.7 mm; DV: −4.3 mm) and the vCA1 (AP: −3.5 mm; ML: 3.7 mm; DV: −3.5 mm). For local infusion of CNO, pedestal guide cannulas (27-gauge, RWD Life Science) were implanted bilaterally 1 mm above the AcbC (AP: +1.6 mm; ML: ±1.2 mm; DV: −3.3 mm). For retrograde tracing, the mice were injected (50 nl min^{-1}) with 100 nl Fluorogold (Fluorochrome, 0.5%) in the AcbC (AP: +1.6 mm; ML: ±1.2 mm; DV: −4.3 mm) and were housed for 3 days before collection of brains for histological analyses[43]. For rabies input tracing, 100 nl of a 1:1 volume mixture of AAV9-EF1α:DIO-his-eGFP-2a-TVA and AAV9-EF1α:DIO-RVG was injected in the AcbC of D1-Cre or D2-Cre mice. Two weeks later, RV*d*G (200 nl) was injected into the AcbC. The rabies-injected mice were then housed in a P2 laboratory for 7 days to allow for RV*d*G spread and dsRed expression.

Engram labeling. For engram cell labeling, we used c-fos-tTA transgenic mice combined with the TRE system and conducted 4 days of conditioning. Two to three weeks before cocaine paired conditioning, c-fos-tTA mice were injected with AAVs in which gene expression was under the control of the tetracycline responsive element (TRE) or Cre-dependent AAV (double *loxP* sites inverse of the AAV) in combination with Cre recombinase under the control of TRE. All the c-fos-tTA mice were maintained using food containing doxycycline (40 mg per kg) before conditioning. After the first saline paired conditioning on day 1, the doxycycline diet was replaced with regular food without doxycycline. Two trials of cocaine paired conditioning were then performed on days 2 and 3. Immediately after cocaine paired conditioning, doxycycline (1 g per kg) diet was provided. Then subsequent saline paired conditioning was performed on day 4.

Open-field task. Spontaneous motor activity was measured in an open-field arena (40 × 40 cm^2) for 30 min. All mice were transferred to the testing room and habituated for 30 min before the test. Tests were conducted with 25 lux luminance in the chamber. The apparatus was cleaned before and between trials. The distance traveled in the arena was quantified using an automated detection system (TopScan, Clever Sys).

Light/dark box task. The light/dark box (46 × 27 × 30 cm) was composed of two compartments: the dark compartment (one-third of the box) and the light compartment (two-thirds of the box). Testing was conducted with 25 lux luminance in the light box. Mice were placed in the center of the light box and allowed full access to both compartments for 6 min. The time mice spent in each compartment was analyzed using an automated detection system (TopScan, Clever Sys)

Elevated O maze task. The O maze was elevated 50 cm above the ground and consisted of two open arms and two closed arms. The mice were placed in the center of the open arm. The sessions were taped using a digital video camera for 6 min, and the time spent in each arm was analyzed using the software Clever System (Clever Sys).

Ex vivo electrophysiology. *Brain tissue preparation.* Living acute brain slice preparation for analyzing synaptic function was performed as previously described[44,45]. After 24 h of conditioning, mice were anesthetized with isoflurane (3.5% induction, 1.5–2% maintenance) and perfused transcardially with 20 ml of ice-cold and oxygenated (95% O_2, 5% CO_2) cutting solution containing the following (in mM): 93 *N*-methyl-D-glucamine diatrizoate, 93 HCl, 2.5 KCl, 1.2 NaH_2PO_4, 30 $NaHCO_3$, 20 HEPES buffer, 25 glucose, 5 sodium ascorbate, 2 thiourea, 3 sodium pyruvate, 10 $MgSO_4$ and 0.5 $CaCl_2$ (pH 7.3–7.4, 295–305 mOsm). The brains were rapidly removed and placed in ice-cold and oxygenated cutting solution. The coronal slices (300 μm) containing the AcbC were prepared using a semiautomatic vibrating blade microtome (HM760V, Thermo) and then transferred to an incubation chamber at 32 °C with the oxygenated cutting solution for 12 min. After the initial recovery period, the slices were then kept at room temperature under constant carbogenation in modified

artificial cerebrospinal fluid (ACSF) that contained (in mM): 94 NaCl, 2.5 KCl, 1.2 NaH_2PO_4, 30 $NaHCO_3$, 20 HEPES, 25 glucose, 5 sodium ascorbate, 2 thiourea, 3 sodium pyruvate, 2 $MgSO_4$ and 2 $CaCl_2$ (pH 7.3–7.4, 295–305 mOsm). For whole-cell patch-clamp recording, the slices were transferred one at a time to the recording chamber and perfused with 32 °C carbogenated recording ACSF containing (in mM): 124 NaCl, 2.5 KCl, 1.2 NaH_2PO_4, 30 $NaHCO_3$, 20 HEPES, 25 glucose, 5 sodium ascorbate, 2 thiourea, 3 sodium pyruvate, 2 $MgSO_4$ and 2 $CaCl_2$ (pH 7.3–7.4, 295–305 mOsm) at a rate of 1.5 ml min^{-1}. Recording neurons were identified visually by location, shape, size and fluorescence.

Spontaneous EPSCs. AMPAR mEPSCs were recorded in randomly selected engram and non-engram neurons (H2B-GFP$^+$ and H2B-GFP$^-$ neurons, respectively) or D1 engram and D1 non-engram neurons (H2B-GFP$^+$ H2B-mCherry$^+$ and H2B-GFP$^+$ H2B-mCherry$^-$ neurons, respectively) in the AcbC using an EPC-10 amplifier (HEKA Elektronik) and pipettes with a resistance of 4–6 MOhm filled with an internal solution containing (in mM): 120 $CeMeSO_3$, 15 CsCl, 8 NaCl, 0.2 EGTA, 10 HEPES, 4 ATP-Mg, 0.3 GTP-Na, 10 tetraethylammonium chloride and 5 QX-314 with the pH adjusted to 7.2 with CsOH. The osmolarity of the internal solution was adjusted to around 290 mmol kg^{-1} with sucrose. The cells were held in voltage-clamp mode at −70 mV for 5 min in the presence of 50 μM D-AP5 (D-2-amino-5-phosphono-valeric acid), 100 μM picrotoxin and 0.5 μM tetrodotoxin. The miniature events were recorded 5 min after entering whole-cell patch-clamp recording mode to allow dialysis of the Cs^+ internal solution for a relatively complete block of the potassium channels in the MSNs. The amplitude and frequency of the mEPSCs were detected and analyzed using MiniAnalysis (Synaptosoft).

Photostimulation of brain slices. A TTL-driven light-emitting diode (Lumen Dynamics) was used to generate photostimuli consisting of a single wide-field blue flash (473 nm, 5-ms duration for vCA1 engram inputs and 1-ms duration for vCA1 excitatory inputs) for photostimulation of ChR2-expressing or oChIEF-expressing terminals. The laser intensity was measured at the focal plane of the slice when delivered through the ×60 water-immersion objective lens (Olympus BX51WI).

AMPA/NMDA EPSC ratio. Brain slices containing the AcbC and ChR2/oChIEF-positive fibers from the vCA1 were chosen for voltage-clamp recording with the same internal solution. The stimulus intensity (0.5–3 mW at 470 nm) was set at a level that could evoke 100–300 pA AMPAR-mediated response with a holding potential at −70 mV. For each AcbC neuron, the same photostimulation intensity and duration was used to record AMPAR and NMDAR EPSCs with 100 μM picrotoxin added to the extracellular solution. The cells were clamped at −70 mV and +40 mV to obtain AMPAR and NMDAR EPSCs in response to photostimulation. The single-pulse photostimulation trials were repeated ten times with an inter-stimulus interval of 15 s. To calculate the A/N ratio, the peak current at −70 mV (AMPA EPSCs) was compared with the current at 50 ms after stimulus onset at +40 mV (NMDA EPSCs). The nontypical A/N ratio (>18) of some AcbC engram cells were excluded.

PPR experiment. PPR experiments were performed on the same cohort of cells with picrotoxin (100 μM) added to the recording ACSF solution. AMPAR EPSCs were evoked by paired photostimuli (50-ms or 100-ms interval) of ChR2/oChIEF-expressing presynaptic axons from the vCA1 and recorded in the AcbC D1 engram or D1 non-engram cells at −70 mV in voltage-clamp mode. The stimulus intensity (0.5–3 mW at 470 nm) was set at a level that the first AMPAR-mediated response was 100–300 pA. PPR was obtained for ten consecutive traces, and only those traces with stable evoked first current responses were used for data analysis. The PPR was calculated as the peak amplitude ratio of the second to the first EPSC.

Action potential firing. To validate the spike fidelity of optogenetic stimulation of ChR2 and the response to stimulation of eNphR3.0, brain slices containing the vCA1 were chosen for current-clamp recording with the internal solution containing (in mM): 105 potassium gluconate, 10 HEPES, 30 KCl, 0.3 EGTA, 4 ATP-Mg, 0.3 GTP-Na and 10 phosphocreatine with the pH adjusted to 7.3 with KOH and the osmolarity to 290 mmol kg^{-1} with sucrose. Blue light (473 nm, 2 mW, 15-ms pulse width for 1 s) was delivered at the frequency of 5 Hz, 10 Hz or 20 Hz to trigger the action potential. Yellow light (593 nm, 2 mW for 2 s) was delivered to eliminate the action potential induced by 100 pA current stimulation. To measure the function and specificity of CNO stimulation of hM3D and hM4D in D1 MSNs, brain slices containing the AcbC were chosen for current-clamp recording. The rheobase was defined as the minimal current amplitude required for firing an action potential with a depolarizing current step (~10 sweeps in 5-pA unit increment) and was measured before and 15 min after CNO (5 μM) application to the bath solution. Individual voltage responses to a 1-s current pulse (100 pA) were also recorded in AcbC engram cells expressing hM4D before and 15 min after CNO (5 μM) application to the bath solution.

During the execution and analysis of the electrophysiological recordings, the investigators were blinded to the genotypes and treatment group of the individual animals. The signals were acquired at 20 kHz and filtered at 2 kHz. The series-resistance was <20 MOhm. Data with series resistance changed by >20% were excluded. mEPSCs were analyzed using Minianalysis and the A/N current ratios and PPRs were analyzed using Clampfit. Values are expressed as the mean ± s.e.m.

In vivo photostimulation. For photostimulation during behavioral assays, a 473-nm (blue light) or 593-nm laser (yellow light) (Shanghai Dream Lasers Technology) was connected to a patch cord with a pair of FC/PC connectors on each end. This patch cord was connected through a fiber optic rotary joint (which allows free rotation of the fiber; Doric Lenses) with another patch cord with a FC/PC connector on one side and ceramic ferrules on the other side (outer diameter of 1.25 mm). The optic fiber implanted in the mouse (200 μm in diameter, 0.37 NA) was connected to the optic patch cord using ceramic mating sleeves (Anilab Software & Instruments). Blue light was delivered at 473 nm in a train of ten 15-ms light pulses at 20 Hz every 10 s for 15 min[6,46]. Yellow light was delivered at 5 mW for 5 min during the CPP retention test[47]. The laser power was measured at the tip of the optic fiber. The laser output was modulated using a Master 8 pulse stimulator (A.M.P.I.).

For the optical LTD experiment, following CPP training, LFS (10 min of 4-ms 473 nm blue light at 1 Hz, 18–20 mW) was delivered in the home cage, and the CPP test and anxiety behavior tests were performed 40 min later. For the optical LTP experiment, following CPP training and extinction training, HFS (six trains of 100 times of 2-ms pulses given at 100 Hz with a 20 s inter-train-interval, 18–20 mW) was delivered to the AcbC in the home cage. The CPP test was then performed 1 day later.

Immunofluorescence. Mice were anesthetized and transcardially perfused with 0.9% saline for 6 min followed by 4% paraformaldehyde (PFA; dissolved in 0.1 M Na_2HPO_4/NaH_2PO_4 buffer (pH 7.5)) for 5 min. Brains were post-fixed in 4% PFA at 4 °C for 4 h and then transferred to 30% sucrose/PBS solution for 3 days. Then brains were sectioned into 30-μm-thick slices, which were then stored in the cryoprotective buffer at −20 °C. For immunofluorescence staining, each slice was placed in PBS and washed three times in PBS, followed by incubation with primary antibody at 4 °C overnight. After rinsing in PBS, the slices were incubated with fluorescence-conjugated secondary antibody at room temperature for 2 h. Finally, slices were coverslipped on anti-quenching mounting medium (Thermo Fisher Scientific). All analyses were performed blinded to the experimental conditions. For primary antibodies, we used antibodies against c-Fos (rabbit, 1:2,000; Santa Cruz, sc-52)[9], NeuN (mouse, 1:500; Millipore, MAB377)[48], RFP (rabbit, 1:500; Rockland, 600-401-379)[9], GFP (chicken, 1:500; Thermo Fisher Scientific, A-10262)[49] and wheat germ agglutinin (rabbit, 1:10,000; Sigma, T4144)[50]. For the secondary antibody, we used Alexa-488 or Cy3 IgG (mouse, rabbit or chicken, 1:50,000; Jackson ImmunoResearch).

High-resolution FISH by RNAscope. Two weeks after anterograde scAAV-Cre injection into the vCA1, the Ai14 mice were perfused intracardiacally with saline then with 4% PFA in 0.1 M Na_2HPO_4/NaH_2PO_4 buffer (pH 7.5) and the brains removed. After post-fixation in 4% PFA for 4 h, the samples were stored in 30% sucrose/PBS for 3 days. FISH was performed on the fixed frozen brain slices (10-μm thick) following the RNAscope procedures (Advanced Cell Diagnostics). In brief, frozen sections (10-μm thick) were cut coronally through the AcbC formation. Sections were thaw-mounted onto Superfrost Plus microscope slides (Fisher Scientific). Sections were incubated with probes against mouse *tdTomato*, *Drd1* and *Drd2* (*tdTomato*, target region 7-1382; *Drd1*, accession no: NM_010076.3, target region 444-1358; *Drd2*, accession no: NM_010077.2, target region 69–1,175) for 2 h at 40 °C with the labeled probe mixture per slide. The nonspecifically hybridized probe was removed by washing the sections in 1× washing buffer at room temperature, followed by Amplifier 1-FL for 30 min, Amplifier 2-FL for 30 min and Amplifier 3-FL for 15 min at 40 °C. Each amplifier was removed by washing with 1× washing buffer for 2 min at room temperature. At least six brain slices from seven male mice were prepared and imaged.

Imaging. Confocal fluorescence images were acquired using a Zeiss LSM510 or a Nikon A1 confocal laser scanning microscope with ×10, ×20, ×25, ×40 or ×60 objectives for imaging stained or autofluorescent neurons. The center of viral infection was taken as the brightest fluorescent point. The tip of the fiber or cannulas was determined by the ~50-μm-thick gliosis generated by the fiber. The slides for FISH were viewed, analyzed and photographed using a Nikon A1 confocal laser scanning microscope and a ×20 objective.

Cell counting. All animals were killed 60 min after memory retrieval or chemogenetic stimulation for immunofluorescence analyses. To characterize the reactivation of engram cells induced by memory retrieval, the number of tdTomato$^+$ or c-Fos-immunoreactive neurons in each brain region were counted from 3–5 coronal slices per mouse (n = 3–5 mice per group; c-fos-tTA×*tetO*-Cre×Ai14 mice). Automated cell counting was conducted using the software Image-Pro Plus 6.0 (IPP). The boundaries of each brain region were outlined as a region of interest (ROI) according to the mouse brain atlas[51], and the area was quantified by applying scale calibration. The number of tdTomato$^+$ or c-Fos$^+$ cells

per section was calculated by applying a threshold above background fluorescence. The number of cells positive for both c-Fos tdTomato was counted manually from the cells selected by IPP. To achieve the counts of tdTomato$^+$ or c-Fos$^+$ cells per mm^2, we divided the number of positive cells by the area of ROI. The percentage of double-positive cells in Supplementary Figs. 1, 3, 6 and 8 was calculated as (c-Fos$^+$ tdTomato$^+$/tdTomato$^+$) × 100 or (c-Fos$^+$ tdTomato$^+$/c-Fos$^+$) × 100. The results of each image from the same group were pooled for further statistical analyses. All counting experiments were conducted blinded to the experimental group.

Spine morphometric analysis. Morphological features such as size, shape and density of dendritic spines were analyzed using single-cell microinjections with Lucifer yellow[52]. Mice were deeply anesthetized and transcardially perfused with ice-cold 1% PFA for 1 min followed by ice-cold 4% PFA for 15 min. The brains were removed and post-fixed overnight in 4% PFA. After post-fixation, the brain was sliced into 200-μm thickness containing the AcbC with a vibratome (HM760V, Thermo) and kept in 0.1 M phosphate buffer at 4 °C. For cell-filling injections, selected brain slices immersed in 0.1 M phosphate buffer were mounted on a tissue stage. Using a micromanipulator, a micropipette loaded with Lucifer yellow dye (Invitrogen L453, 5% solution in PBS, pH 7.4) was used to impale the cell body and deliver the dye with a continuous 2 nA current for 5 min. Then the brain slices were mounted on slides using Lerner Aqua-Mount (13800, Thermo) and imaged using an Olympus confocal laser scanning microscope (FV1000, ×60 oil objective). Spines on secondary dendrites were traced and analyzed. To determine the spine size, ~30 neurons (from 6 mice) were measured. Spine types were classified as previously described[53]. The spine density of each type was expressed as the number of spines per 10 μm of dendrite. The heads of spines were measured by taking the maximal width of the spine head perpendicular to the axis along the spine neck. The spine density and spine head width were analyzed using NeuronStudio[54,55]. During analysis of the fluorescence images, the investigators were blinded to the genotypes and treatment group of the individual animals.

Fiber photometry recording. AAV-EF1α:DIO-GCaMP6s and AAV-TRE-ChR2-mCherry were individually injected into the AcbC and the vCA1. An optical fiber (outer diameter of 200 μm, 0.48 NA, Hangzhou Newdoon Technology) was implanted unilaterally into the AcbC (AP: +1.6 mm; ML: 1.2 mm; DV: −4.3 mm), and another one was ipsilaterally implanted into the vCA1 (AP: −3.5 mm; ML: 3.7 mm; DV: −3.5 mm). The fiber photometry device was developed by Luo's Lab[56,57]. The laser power was adjusted at the tip of optical fiber to the low level of 10–20 μW to minimize bleaching. The GCaMP fluorescence was collected and converted to voltage signals. The analog voltage signals were digitalized at 100 Hz and recorded using the software Fiber photometry (Thinker Tech Nanjing Biotech). Photometry data were further analyzed using Matlab. The data were segmented based on behavioral events within individual trials. We derived the values of fluorescence change ($\Delta F/F$) by calculating $(F - F_0)/F_0$, where F_0 is the baseline fluorescence signal averaged over a 2-s long control time window preceding the trigger events. $\Delta F/F$ values are presented as heatmaps or average plots, with the shaded area indicating the standard error of the mean.

Quantification and statistical analyses. No statistical methods were used to predetermine sample sizes, but our sample sizes were based on prior literature and best practices in the field[58,59]. All experimental data are shown as the mean ± s.e.m. and plotted using Graphpad Prism v.7. All the statistical analyses were performed using Stata 14, SPSS 20 and SigmaPlot 12.5. Comparisons of distribution data between two groups were analyzed using Kolmogorov–Smirnov tests. Single-variable differences were detected using two-tailed unpaired (as noted) Student's *t*-tests or one-way analysis of variance (ANOVA). Multiple group comparisons were assessed using one-way or two-way ANOVA, followed by post-hoc Bonferroni's test when significant main effects or interactions were detected. In detail, immunofluorescence data were analyzed using *t*-tests, one-way ANOVA or Kruskal–Wallis one-way ANOVA on ranks if the data were non-normally distributed. Group differences of behavioral tests were detected using two-way repeated-measures (RM) ANONA or Friedman's two-way RM ANOVA by ranks if the data were non-normally distributed, followed by Bonferroni's post-hoc tests with sessions as a within-subjects factor and drug treatment or virus as a between-subjects factor. The electrophysiological data were tested for significance using either one-way or two-way ANOVA, or Kruskal–Wallis one-way ANOVA on ranks if the data were non-normally distributed, followed by Bonferroni's post-hoc tests with sessions as a within-subjects factor and treatment as a between-subjects factor. Full statistical analyses corresponding to each figure can be found in Supplementary Table 1.

Reporting Summary. Further information on research design is available in the Nature Research Reporting Summary linked to this article.

Data availability

The data that support the findings of this study are available from the corresponding authors upon reasonable request.

Code availability

Custom Matlab code is available on reasonable request from L.M.

References

43. Mondello, S. E., Jefferson, S. C., O'Steen, W. A. & Howland, D. R. Enhancing Fluorogold-based neural tract tracing. *J. Neurosci. Methods* **270**, 85–91 (2016).
44. Ting, J. T., Daigle, T. L., Chen, Q. & Feng, G. Acute brain slice methods for adult and aging animals: application of targeted patch clamp analysis and optogenetics. *Methods Mol. Biol.* **1183**, 221–242 (2014).
45. Zhao, S. et al. Cell type-specific channelrhodopsin-2 transgenic mice for optogenetic dissection of neural circuitry function. *Nat. Methods* **8**, 745–752 (2011).
46. Redondo, R. L. et al. Bidirectional switch of the valence associated with a hippocampal contextual memory engram. *Nature* **513**, 426–430 (2014).
47. Lee, J., Finkelstein, J., Choi, J. Y. & Witten, I. B. Linking cholinergic interneurons, synaptic plasticity, and behavior during the extinction of a cocaine-context association. *Neuron* **90**, 1071–1085 (2016).
48. Huang, B. et al. β-Arrestin-biased beta-adrenergic signaling promotes extinction learning of cocaine reward memory. *Sci. Signal.* **11**, eaam5402 (2018).
49. Kitamura, T. et al. Engrams and circuits crucial for systems consolidation of a memory. *Science* **356**, 73–78 (2017).
50. Dobi, A., Margolis, E. B., Wang, H. L., Harvey, B. K. & Morales, M. Glutamatergic and nonglutamatergic neurons of the ventral tegmental area establish local synaptic contacts with dopaminergic and nondopaminergic neurons. *J. Neurosci.* **30**, 218–229 (2010).
51. Franklin, K. B. J. & Paxinos, G. *The Mouse Brain in Stereotaxic Coordinates* (Academic Press, 2013).
52. Dumitriu, D., Rodriguez, A. & Morrison, J. H. High-throughput, detailed, cell-specific neuroanatomy of dendritic spines using microinjection and confocal microscopy. *Nat. Protoc.* **6**, 1391–1411 (2011).
53. Yuste, R. & Bonhoeffer, T. Genesis of dendritic spines: insights from ultrastructural and imaging studies. *Nat. Rev. Neurosci.* **5**, 24–34 (2004).
54. Rodriguez, A., Ehlenberger, D. B., Dickstein, D. L., Hof, P. R. & Wearne, S. L. Automated three-dimensional detection and shape classification of dendritic spines from fluorescence microscopy images. *PLoS One* **3**, e1997 (2008).
55. Rodriguez, A., Ehlenberger, D. B., Hof, P. R. & Wearne, S. L. Rayburst sampling, an algorithm for automated three-dimensional shape analysis from laser scanning microscopy images. *Nat. Protoc.* **1**, 2152–2161 (2006).
56. Li, Y. et al. Serotonin neurons in the dorsal raphe nucleus encode reward signals. *Nat. Commun.* **7**, 10503 (2016).
57. Guo, Q. et al. Multi-channel fiber photometry for population neuronal activity recording. *Biomed. Opt. Express* **6**, 3919–3931 (2015).
58. Gunaydin, L. A. et al. Natural neural projection dynamics underlying social behavior. *Cell* **157**, 1535–1551 (2014).
59. Martin-Fernandez, M. et al. Synapse-specific astrocyte gating of amygdala-related behavior. *Nat. Neurosci.* **20**, 1540–1548 (2017).

Acknowledgements

This research was supported by grants from the National Natural Science Foundation of China (31430033, 31930046 and 91632307 to L.M., 31771176 and 31571036 to X.L.), the Ministry of Science and Technology (2015CB553501 to L.M.), the Shanghai Municipal Science and Technology Major Project (2018SHZDZX01 to L.M.) and the ZJLab.

Author contributions

L.M., X.L., Y.Z. and H.Z designed the experiments. H.Z., Y.Z., X.C. and Z.L. performed the behavioral experiments. Y.Z. and X.L. designed the electrophysiology experiments and Y.Z. performed most of the electrophysiological experiments. H.Z., Z.L. and X.C. assisted with the electrophysiology experiments. Figure 1b and Supplementary Fig. 8j,k were prepared by Z.L.. H.Z., C.M. and X.C. processed and analyzed the electrophysiological data. H.Z., Y.Z. and X.L. performed viral injections, brain preparation, imaging and analysis. Z.L., X.S., C.M., Z.T. and E.Y. assisted with viral injections and cocaine conditioning. B.H. performed molecular cloning. L.M. and X.L. supervised the project. L.M., X.L. and Y.Z. wrote the paper.

Competing interests

The authors declare no competing interests.

Additional information

Supplementary information is available for this paper at https://doi.org/10.1038/s41593-019-0524-y.

Correspondence and requests for materials should be addressed to X.L. or L.M.

Peer review information *Nature Neuroscience* thanks Denise Cai, Yan Dong, and the other, anonymous, reviewer(s) for their contribution to the peer review of this work.

Reprints and permissions information is available at www.nature.com/reprints.

nature research

Corresponding author(s): DBPR NN-A65830-T

Last updated by author(s): Sep 12, 2019

Reporting Summary

Nature Research wishes to improve the reproducibility of the work that we publish. This form provides structure for consistency and transparency in reporting. For further information on Nature Research policies, see Authors & Referees and the Editorial Policy Checklist.

Statistics

For all statistical analyses, confirm that the following items are present in the figure legend, table legend, main text, or Methods section.

n/a	Confirmed
☐	☒ The exact sample size (*n*) for each experimental group/condition, given as a discrete number and unit of measurement
☐	☒ A statement on whether measurements were taken from distinct samples or whether the same sample was measured repeatedly
☐	☒ The statistical test(s) used AND whether they are one- or two-sided *Only common tests should be described solely by name; describe more complex techniques in the Methods section.*
☐	☒ A description of all covariates tested
☐	☒ A description of any assumptions or corrections, such as tests of normality and adjustment for multiple comparisons
☐	☒ A full description of the statistical parameters including central tendency (e.g. means) or other basic estimates (e.g. regression coefficient) AND variation (e.g. standard deviation) or associated estimates of uncertainty (e.g. confidence intervals)
☐	☒ For null hypothesis testing, the test statistic (e.g. *F*, *t*, *r*) with confidence intervals, effect sizes, degrees of freedom and *P* value noted *Give P values as exact values whenever suitable.*
☒	☐ For Bayesian analysis, information on the choice of priors and Markov chain Monte Carlo settings
☒	☐ For hierarchical and complex designs, identification of the appropriate level for tests and full reporting of outcomes
☒	☐ Estimates of effect sizes (e.g. Cohen's *d*, Pearson's *r*), indicating how they were calculated

Our web collection on statistics for biologists contains articles on many of the points above.

Software and code

Policy information about availability of computer code

Data collection	Labview:Custom fiber photometry data collection and analysis, as previously described in Guo QC et al., Biomedical Optics Express 2015; Li Y et al., Nature communication 2016. PatchMaster (HEKA): Recording of the current and voltage signals for slice electrophysiology Ethovision XT 8: Data collection for Open field, light/dark system and elevated O-maze behavior tests Zeiss LSM510, Nikon A1 or Olympus FV1000: Confocal fluorescence imaging
Data analysis	MATLAB R2018b:Custom fiber photometry data analysis, as previously described in Eban-Rothschild et al., Nat. Neurosci. 2016. pCLAMP10 (Molecular Devices) : AMPAR and NMDAR EPSC analysis . MiniAnal (Synaptosoft http://www.synaptosoft.com/MiniAnalysis/): mEPSC analysis. NeuroStudio (CNIC, Mount Sinai School of Medicine http://research.mssm.edu/cnic/help/ns/index.html): Spine morphometric analysis. Clever System software: Data analysis for Open field, light/dark system and elevated O-maze behavior tests Image-Pro Plus 6.0 (IPP): Cell counting Stata 14, SPSS 20, and SigmaPlot 12.5: All Statistical analysis Graphpad Prism version 7: Plotting

For manuscripts utilizing custom algorithms or software that are central to the research but not yet described in published literature, software must be made available to editors/reviewers. We strongly encourage code deposition in a community repository (e.g. GitHub). See the Nature Research guidelines for submitting code & software for further information.

Data

Policy information about availability of data

All manuscripts must include a data availability statement. This statement should provide the following information, where applicable:

- Accession codes, unique identifiers, or web links for publicly available datasets
- A list of figures that have associated raw data
- A description of any restrictions on data availability

The authors declare that all data supporting the findings of this study are available

Field-specific reporting

Please select the one below that is the best fit for your research. If you are not sure, read the appropriate sections before making your selection.

☒ Life sciences ☐ Behavioural & social sciences ☐ Ecological, evolutionary & environmental sciences

For a reference copy of the document with all sections, see nature.com/documents/nr-reporting-summary-flat.pdf

Life sciences study design

All studies must disclose on these points even when the disclosure is negative.

Sample size	No statistical methods were used to pre-determine sample sizes but our sample sizes are based on prior literature and best practices in the field (Gunaydin, L.A., et al. 2014, Martin-Fernandez, M., et al. 2017)
Data exclusions	The criterion was established before data collection. In the CPP tests, mice that spent > 65 % (> 585 s) or < 35 % (< 315 s) of the total time (900 s) in one side were eliminated from subsequent CPP experiments. For in vitro electrophysiological recordings, data with series resistance changed by >20% were excluded.
Replication	All the experiments were reliably reproduced for two to three batches.
Randomization	Mice were randomly assigned to experimental groups, and all groups consisted of age- and sex-matched littermates.
Blinding	The retention phases of CPP were taped by a digital video camera, and a trained observer blind to the genotype and treatment recorded the time spent exploring the two chambers according to the video by a stopwatch. For execution and analysis of the electrophysiological recordings and confocal imaging, the investigators were blind to the genotypes and treatments of the individual animals.

Reporting for specific materials, systems and methods

We require information from authors about some types of materials, experimental systems and methods used in many studies. Here, indicate whether each material, system or method listed is relevant to your study. If you are not sure if a list item applies to your research, read the appropriate section before selecting a response.

Materials & experimental systems

n/a	Involved in the study
☐	☒ Antibodies
☒	☐ Eukaryotic cell lines
☒	☐ Palaeontology
☐	☒ Animals and other organisms
☒	☐ Human research participants
☒	☐ Clinical data

Methods

n/a	Involved in the study
☒	☐ ChIP-seq
☒	☐ Flow cytometry
☒	☐ MRI-based neuroimaging

Antibodies

Antibodies used	Primary antibodies used: Rabbit polyclonal anti-c-Fos: Santa Cruz sc-52, 1:2000, Lot: F1715 Mouse anti-NeuN: Millipore MAB377, 1:500, Lot: 2716741 Rabbit polyclonal anti-Wheat Germ Agglutinin: Sigma-Aldrich T4144, 1:10000 Rabbit polyclonal anti-RFP: Rochland 600-401-379, 1:500, Lot: 39707 Chicken polyclonal anti-GFP: Thermo Fisher Scientific A-102602, 1:500, Lot: GR3190550-8 Secondary antibodies used: Goat anti-rabbit, Alexa-488: Jackson Immuno Research 111-545-144, 1:50000 Goat anti-rabbit, Cy3: Jackson ImmunoResearch 111-165-144, 1:50000

Donkey anti-chicken, Alexa-488: Jackson ImmunoResearch 703-545-155, 1:50000
Donkey anti-mouse, Alexa-488: Jackson ImmunoResearch 715-545-150, 1:50000

Validation

Primary antibodies:
anti-c-Fos: PMID: 26023136
anti-NeuN: PMID: 29317519
anti-Wheat Germ Agglutinin: PMID: 20053904
anti-RFP: PMID: 26023136
anti-GFP: PMID: 28386011

Animals and other organisms

Policy information about studies involving animals; ARRIVE guidelines recommended for reporting animal research

Laboratory animals	We used adult (8-10 week old) male mice on C57BL/6J background, of several strains described in Methods: wild-type C57BL/6: Slaccsas Lab N/A c-Fos-tTA: Jackson Laboratory #008344 tetO-cre: Jackson Laboratory #006234 tetO-H2B-GFP: Jackson Laboratory #005104 Gt(ROSA)26Sortm14(CAG-tdTomato)Hze (Ai14): Jackson Laboratory #007914 Drd1-cre: The Mutant Mouse Resource and Research Center #030989-UCD-HEMI Drd2-cre: The Mutant Mouse Resource and Research Center #032108-UCD-HEMI Drd2-EGFP: The Mutant Mouse Resource and Research Center #000230-UNC-HEMI
Wild animals	This study did not involve wild animals
Field-collected samples	This study did not involve samples collected from the field.
Ethics oversight	Experimental procedures were approved by Animal Care and Use Committee of Shanghai Medical College of Fudan University.

Note that full information on the approval of the study protocol must also be provided in the manuscript.